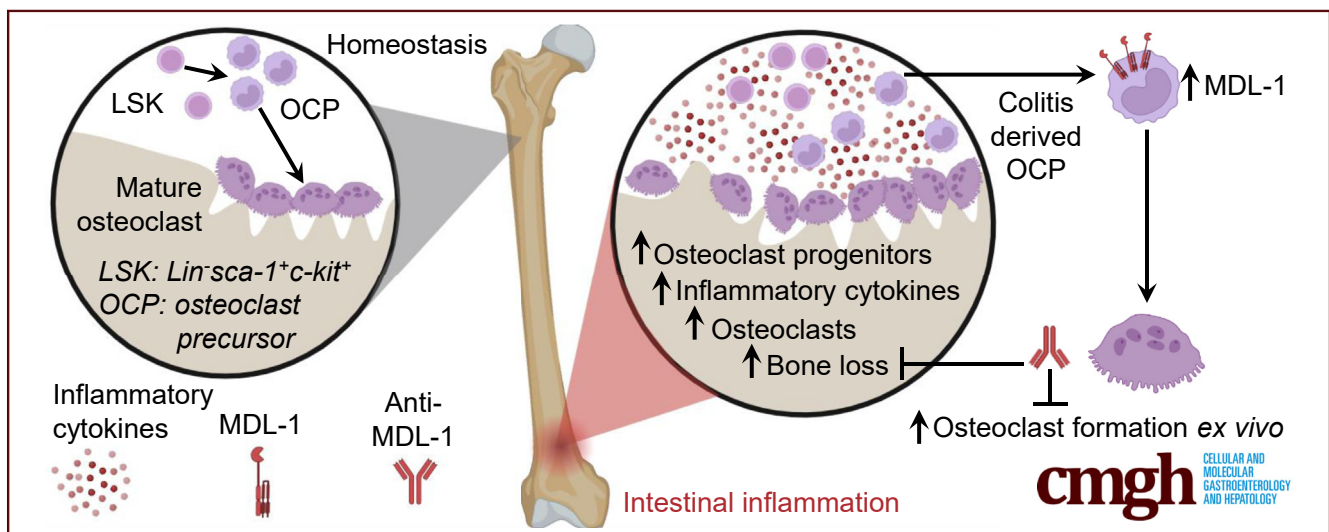


ORIGINAL RESEARCH

Intestinal Inflammation Promotes MDL-1⁺ Osteoclast Precursor Expansion to Trigger Osteoclastogenesis and Bone Loss

Christopher T. Peek,¹ Caleb A. Ford,² Kara R. Eichelberger,³ Justin Jacobse,^{1,4} Teresa P. Torres,¹ Damian Maseda,^{1,10} Yvonne L. Latour,¹ M. Blanca Piazuelo,^{4,6} Joshua R. Johnson,⁹ Mariana X. Byndloss,^{1,5} Keith T. Wilson,^{1,4,5,6,7} Jeffrey C. Rathmell,^{1,5,6,8} Jeremy A. Goettel,^{1,4,5,6} and James E. Cassat^{1,2,3,5,6,8,9}

¹Department of Pathology, Microbiology, and Immunology, Vanderbilt University Medical Center, Nashville, Tennessee; ²Department of Biomedical Engineering, Vanderbilt University, Nashville, Tennessee; ³Department of Pediatrics, Division of Pediatric Infectious Diseases, Vanderbilt University Medical Center, Nashville, Tennessee; ⁴Division of Gastroenterology, Hepatology, and Nutrition, Department of Medicine, Vanderbilt University Medical Center, Nashville, Tennessee; ⁵Vanderbilt Institute for Infection, Immunology, and Inflammation, Vanderbilt University Medical Center, Nashville, Tennessee; ⁶Center for Mucosal Inflammation and Cancer, Vanderbilt University Medical Center, Nashville, Tennessee; ⁷Veterans Affairs Tennessee Valley Healthcare System, Nashville, Tennessee; ⁸Vanderbilt Center for Immunobiology, Vanderbilt University Medical Center, Nashville, Tennessee; ⁹Vanderbilt Center for Bone Biology, Vanderbilt University Medical Center, Nashville, Tennessee; and ¹⁰Department of Dermatology, University of Pennsylvania, Philadelphia, Pennsylvania



SUMMARY

This work utilizes multiple models of intestinal inflammation to demonstrate a pathologic expansion of osteoclast precursors associated with bone loss during intestinal inflammation. Data from this study highlight the feasibility of targeting a pro-osteoclastogenic co-receptor to ameliorate colitis-associated bone loss.

BACKGROUND & AIMS: Inflammatory bowel disease (IBD) is characterized by severe gastrointestinal inflammation, but many patients experience extra-intestinal disease. Bone loss is one common extra-intestinal manifestation of IBD that occurs through dysregulated interactions between osteoclasts and osteoblasts. Systemic inflammation has been postulated to contribute to bone loss, but the specific pathologic mechanisms

have not yet been fully elucidated. We hypothesized that intestinal inflammation leads to bone loss through increased abundance and altered function of osteoclast progenitors.

METHODS: We used chemical, T cell driven, and infectious models of intestinal inflammation to determine the impact of intestinal inflammation on bone volume, the skeletal cytokine environment, and the cellular changes to pre-osteoclast populations within bone marrow. Additionally, we evaluated the potential for monoclonal antibody treatment against an inflammation-induced osteoclast co-receptor, myeloid DNAX activation protein 12-associating lectin-1 (MDL-1) to reduce bone loss during colitis.

RESULTS: We observed significant bone loss across all models of intestinal inflammation. Bone loss was associated with an increase in pro-osteoclastogenic cytokines within the bone and an expansion of a specific Cd11b^{hi}/Ly6C^{hi} osteoclast precursor

(OCP) population. Intestinal inflammation led to altered OCP expression of surface receptors involved in osteoclast differentiation and function, including the pro-osteoclastogenic co-receptor MDL-1. OCPs isolated from mice with intestinal inflammation demonstrated enhanced osteoclast differentiation *ex vivo* compared to controls, which was abrogated by anti-MDL-1 antibody treatment. Importantly, *in vivo* anti-MDL-1 antibody treatment ameliorated bone loss during intestinal inflammation.

CONCLUSIONS: Collectively, these data implicate the pathologic expansion and altered function of OCPs expressing MDL-1 in bone loss during IBD. (*Cell Mol Gastroenterol Hepatol* 2022; 14:731–750; <https://doi.org/10.1016/j.jcmgh.2022.07.002>)

Keywords: Inflammatory Bowel Disease; MDL-1; Osteoclast.

Inflammatory bowel disease (IBD) is hallmarked by severe gastrointestinal inflammation that is mediated, in part, by aberrant innate and adaptive immune responses. Additionally, the inflammation that patients with Crohn's disease and ulcerative colitis experience frequently impacts extra-intestinal sites. Up to 40% of patients with IBD experience extra-intestinal symptoms, which can occur in nearly every tissue type before, concurrent with, or after the onset of colitis.^{1–3} Musculoskeletal disease is among the most common extra-intestinal manifestations of IBD and ultimately confers a 40% increased risk of osteoporotic fracture compared with the general population.⁴ Although nutritional status and medication use are potential contributors to colitis-associated bone loss, accumulating evidence supports a crucial role for inflammation in driving bone loss during IBD. For example, patients with normal vitamin D and calcium levels can still experience IBD-associated bone loss, as can patients who have not yet started IBD treatment.^{3,5,6} Moreover, cytokine blocking therapy partially prevents bone loss in patients with IBD and correlates with improved serum markers of bone resorption.^{7,8} One potential mechanism by which IBD-associated inflammation triggers bone loss is through the actions of inflammatory cytokines on skeletal cells.

The goal of this study was to further define how gastrointestinal inflammation leads to bone loss through impacts on osteoclasts. Osteoclasts are multi-nucleated, myeloid lineage cells capable of resorbing bone. Osteoclast differentiation and survival require receptor activator of nuclear factor kappa-B ligand (RANKL) and macrophage colony stimulating factor (M-CSF) signaling and are further regulated by the RANKL decoy receptor, osteoprotegerin (OPG). Multiple myeloid cell types across various tissue sources can differentiate into osteoclasts in the presence of M-CSF and RANKL. Cells capable of differentiating into osteoclasts include LSK (lineage negative, Sca-1⁺, c-Kit⁺) hematopoietic stem cells (HSCs), monocytes, and dendritic cells.^{9–12} Patients with IBD-associated bone loss exhibit altered RANKL/OPG levels and elevated serum markers of bone turnover, suggesting that osteoclast differentiation and activity are increased in this patient population.^{8,13}


Importantly, the isolated binding of M-CSF and RANKL to their cognate receptors is insufficient to induce osteoclast

formation *in vivo* or *in vitro* without the coordinated signaling of several osteoclast co-receptors.¹⁴ Activating co-receptors promote osteoclast formation through intracellular immunoreceptor tyrosine-based activation motif (ITAM)-signaling adaptors.¹⁴ Intracellular ITAM-signaling adaptors, such as DNAX activation protein 12 (DAP-12) or FcεR1 gamma chain, pair with receptors capable of binding membrane-bound and extracellular ligands to transduce ITAM activation and trigger calcium fluxes that initiate osteoclast formation.¹⁵ Myeloid DAP-12-associating lectin-1 (MDL-1; also known as C-type lectin domain family 5, member A or CLEC5A) and triggering receptor expressed on myeloid cells 2 (TREM2) are examples of DAP-12-associating osteoclast co-receptors, whereas FcεR1 gamma chain-associated co-receptors include osteoclast activating receptor (OSCAR) and paired-immunoglobulin-like receptor A (PIR-A). Although some ligand-receptor pairs have been identified for these osteoclast co-receptors, many remain poorly described.

Osteoclasts and their precursors are exquisitely sensitive to inflammatory cytokines (eg, interleukin [IL]-1 and tumor necrosis factor-alpha [TNF-α]), chemokines (eg, sphingosine-1-phosphate and CCL-2), and colony stimulating factors (eg, granulocyte colony-stimulating factor [G-CSF]) that can further modulate osteoclast differentiation and function.^{16–21} The sensitivity of osteoclasts to the surrounding cytokine milieu is in part driven by cross regulation of ITAM-associated osteoclast co-receptors. G-CSF, IL-23, and TNF-α have been previously reported to enhance MDL-1 expression on myeloid cells and increase osteoclast formation *in vitro* and *in vivo*.^{22–24} Activation of MDL-1 on myeloid cells, in turn, results in the robust release of RANTES/CCL-5, CXCL-10, TNF-α, and G-CSF.^{22,23,25,26} Several of these osteoclastogenic cytokines are crucial to both the intestinal and extra-intestinal pathogenesis of IBD.^{27–29}

Previous studies have examined bone loss in murine models of colitis, including chemical injury, genetic, T cell

Abbreviations used in this paper: ACT, adoptive T cell transfer; ANOVA, analysis of variance; ASBMR, American Society for Bone and Mineral Research; BV/TV, bone volume over total volume; CFU, colony-forming unit; DAP-12, DNAX activation protein 12; DSS, dextran sulfate sodium; FACS, fluorescent automated cell sorting; G-CSF, granulocyte colony-stimulating factor; HSCs, hematopoietic stem cells; H&E, hematoxylin and eosin; IBD, inflammatory bowel disease; IL, interleukin; ITAM, immunoreceptor tyrosine-based activation motif; LSK, lineage negative, Sca-1⁺, c-Kit⁺; M-CSF, macrophage colony stimulating factor; MDL-1, myeloid DAP-12-associating lectin-1; micro CT, micro-computed tomography; OCP, osteoclast precursor; OPG, osteoprotegerin; OSCAR, osteoclast activating receptor; PBS, phosphate buffered saline; PIR-A, paired-immunoglobulin-like receptor A; RANKL, receptor activator of nuclear factor kappa-B ligand; RISK, Risk Stratification and Identification of Immunogenetic and Microbial Markers of Rapid Disease Progression in Children With Crohn's Disease; STM, *Salmonella enterica* subspecies *enterica* serovar Typhimurium; TNF-α, tumor necrosis factor-alpha; TRAP, tartrate-resistant acid phosphatase; TREM2, triggering receptor expressed on myeloid cells 2; TSSS, type III secretion system; WT, wild-type.

 Most current article

© 2022 The Authors. Published by Elsevier Inc. on behalf of the AGA Institute. This is an open access article under the CC BY-NC-ND license (<http://creativecommons.org/licenses/by-nc-nd/4.0/>).

2352-345X

<https://doi.org/10.1016/j.jcmgh.2022.07.002>

mediated, and infection models.^{30–44} However, the mechanisms by which gastrointestinal inflammation promotes bone loss through effects on skeletal cells are still being uncovered. We hypothesized that changes in osteoclast progenitor populations during intestinal inflammation contribute to IBD-associated bone loss. Using chemical injury, infectious, and adoptive T cell transfer models of gastrointestinal inflammation, we discovered that an increase in the surface expression of the osteoclast co-receptor MDL-1 on Cd11b^{-/lo}Ly6C^{hi} osteoclast precursors (OCPs) is associated with enhanced osteoclastogenesis and significant bone loss during colitis. Anti-MDL-1 antibody treatment was sufficient to blunt ex vivo enhanced osteoclast formation in OCPs derived from mice with chemical colitis. Finally, in vivo, anti-MDL-1 was effective in limiting bone loss during chemically induced colitis.

Results

Intestinal Inflammation Results in Trabecular Bone Loss

To investigate bone loss during colitis, we first induced gastrointestinal inflammation via chemical injury with dextran sulfate sodium (DSS). Mice were given 3% DSS orally for 1 week followed by a 1-week recovery period. As expected, DSS treatment led to weight loss and colonic injury (Figure 1, A–B). We evaluated bone loss using micro-computed tomography (micro CT). DSS-treated mice demonstrated a 37% reduction ($P < .0001$) in trabecular bone volume over total volume (BV/TV) 14 days following DSS treatment compared with controls (Figure 1, C–D). Trabecular bone loss was associated with a significant reduction in trabecular bone thickness ($P < .0001$), increased trabecular separation ($P < .01$), loss of trabeculae ($P < .05$), and reduced connective density ($P < .05$) (Figure 1, E–H). To evaluate if this bone loss was preceded by changes in the number of osteoclasts, we performed histomorphometry on tartrate-resistant acid phosphatase (TRAP)-stained femur sections. Histologically, we observed a significant increase in osteoclast number per bone surface ($P < .05$), but not osteoclast surface per bone surface ($P = .06$) at day 7 following DSS administration (Figure 1, I–K). These results indicate that trabecular bone loss occurs during a chemical injury model of intestinal inflammation, and that an increase in osteoclast number precedes trabecular bone loss.

Next, we tested whether alternative models of intestinal inflammation are associated with bone loss. First, we utilized an adoptive T cell transfer (ACT) model of colitis where *Rag1*^{-/-} mice are injected with naïve CD4⁺CD25⁻CD45RB^{hi} T cells and subsequently develop colitis.⁴⁵ Mice subjected to ACT experienced colonic injury and bone loss, with a 65% reduction in trabecular BV/TV ($P < .001$) (Figure 2, A and Figure 3, A). We subsequently investigated if 2 infectious models of intestinal inflammation were associated with bone loss. Mice subjected to infectious colitis following inoculation of *Citrobacter rodentium* developed intestinal inflammation, bacterial colonization, and significant trabecular bone loss ($P < .05$) compared

with mock infection (Figure 2, B and Figure 3, B). We next infected mice with either wild-type (WT) *Salmonella enterica* subspecies *enterica* serovar Typhimurium (STm), or an attenuated STm mutant, $\Delta invA::tetRA \Delta spiB::KSAC$ (*invA spiB*), that lacks functional type III secretion systems 1 and 2 (T3SS1 and T3SS2) and does not induce robust intestinal inflammation.⁴⁶ We observed that mice infected with WT STm developed cecal injury, bacterial colonization, and significant trabecular bone loss ($P < .01$) compared with infection with *invA spiB* (Figure 2, C and Figure 3, C). Importantly, both *C. rodentium* and WT STm infection led to bacterial colonization, intestinal inflammation, and bone loss in the absence of significant changes in weight over the course of the infection (Figure 2, B–C). Taken together, these data indicate that trabecular bone loss occurs during T cell driven and infectious models of intestinal inflammation. The data further show that bone loss during STm-infectious colitis is driven by pathogen virulence programs that promote intestinal inflammation.

Intestinal Inflammation Alters Cytokine Abundance Within the Bone

We hypothesized that bone loss during intestinal inflammation was mediated, in part, by alterations in the cytokine milieu within the bone microenvironment. To test this hypothesis, we performed multiplexed cytokine analysis on homogenized femurs from mice with or without colitis. We observed significant increases in several chemokines and inflammatory cytokines, including G-CSF, TNF- α , IL-12p40, MCP-1/CCL-2, RANTES/CCL-5, and keratinocyte-derived chemokine/CXCL1 across multiple colitis models (Figure 3, D and Figure 4). Notably, G-CSF, IL-12p40, and TNF- α were among the most significantly increased cytokines across DSS, ACT, *Citrobacter rodentium*, and STm-induced colitis (Figure 3, D). Additional cytokines, including IL-23 and CCL-20, were also significantly elevated during DSS-induced colitis (Figure 4). These data suggest that cells within the murine bone environment experience an altered cytokine milieu in the setting of intestinal inflammation.

Intestinal Inflammation Results in the Expansion of Pre-osteoclast Populations

Because we observed that multiple models of intestinal inflammation dramatically increased G-CSF, which potently regulates myelopoiesis, we evaluated changes in myeloid-derived osteoclast progenitor populations during colitis. Specifically, we examined LSK HSCs, Cd11b^{-/lo}Ly6C^{hi} OCPs, and monocytes. Monocytes and LSK cells were gated according to Figure 5. OCPs were gated as demonstrated in Figure 6, A. We observed a significant increase in the relative abundance of monocytes, LSKs, and OCPs within the bone marrow across chemical and infectious models of intestinal inflammation (Figure 7, A–C). During ACT-induced intestinal inflammation, we observed an increase in LSK and OCPs, but not monocytes (Figure 7, D). Collectively, these data reveal that intestinal inflammation drives an expansion of pre-osteoclast populations.

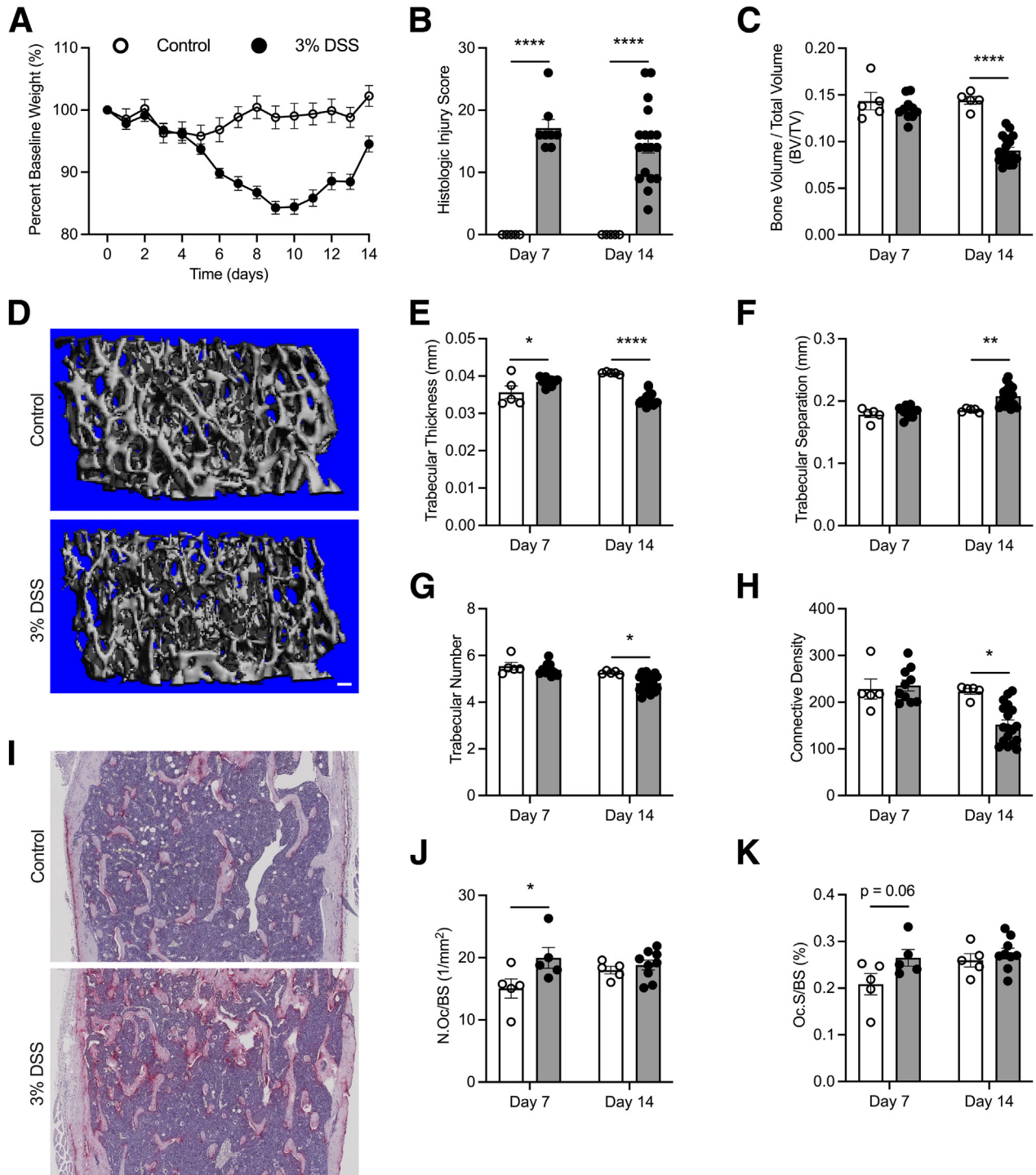


Figure 1. DSS colitis leads to trabecular bone loss. Mice were administered 3% DSS (closed circles) or water (control, open circles) for 7 days, after which time DSS was switched to water. (A) Percent baseline weight of mice with or without DSS colitis. (B) Histologic injury score of H&E-stained colons on days 7 and 14 following DSS administration. (C–H) Micro CT analysis of control (open circles) and DSS-treated (closed circles) formalin-fixed femurs for trabecular BV/TV (C) representative 3-dimensional reconstruction of trabecular bone from mice with or without colitis at day 14 (D) trabecular thickness (E) trabecular separation (F) trabecular number (G) and connective density (H) at day 7 or 14 following DSS treatment. Scale bar = 100 μ m. (I–K) Fixed femurs were paraffin-embedded, sectioned, and stained for TRAP. (I) Representative image of TRAP-stained femurs from mice with or without colitis at day 7 (original magnification = 10 \times). (J) Number of osteoclasts per bone surface (N.Oc/BS). (K) Osteoclast surface per bone surface (Oc.S/BS). Error bars represent mean \pm standard error of the mean. Data analyzed via 2-way ANOVA with Sidák multiple comparisons test. $n = 5$ –18 mice per group. Post-hoc tests were only performed for significant ($P < .05$) ANOVAs. For (J) data analysis by 2-way ANOVA indicated that only DSS treatment ($P = .02$), but not time ($P = .4$) or interaction of these variables ($P = .09$) was significant. Post-hoc Sidák's multiple comparisons test demonstrated an adjusted $P = .02$ at day 7 between control and DSS treated mice. For (K) by 2-way ANOVA, only DSS treatment ($P = .04$), but not time ($P = .08$), or interaction of these variables ($P = .21$) was significant. Post-hoc Sidák's multiple comparisons test demonstrated an adjusted $P = .06$ at day 7 between control and DSS-treated mice. * $P < .05$; ** $P < .01$; **** $P < .0001$.

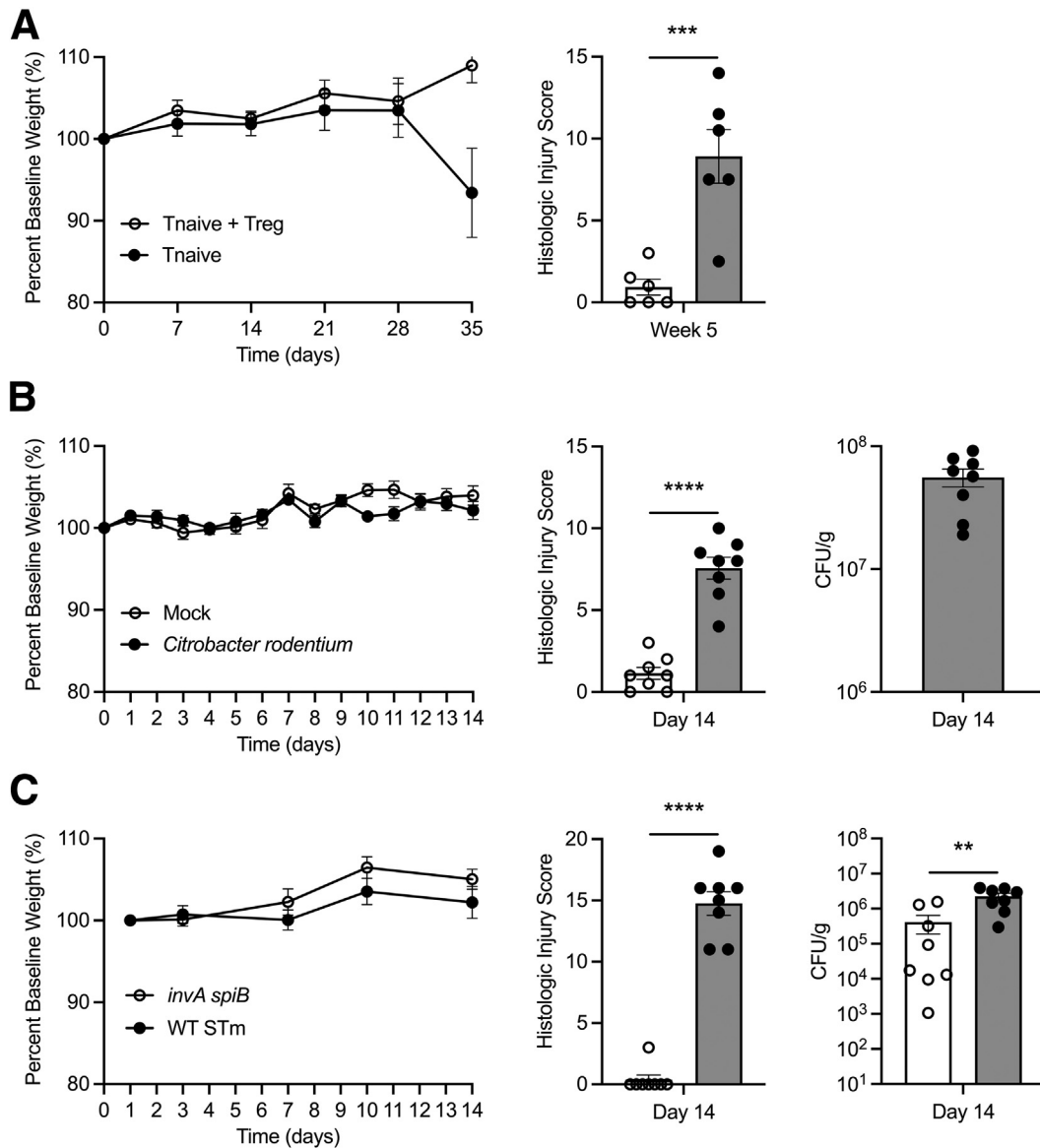


Figure 2. Evidence of histologic injury in mice with adoptive T cell transfer or infection-induced colitis. (A) *Rag1*^{-/-} mice were injected with 5.0×10^5 CD4⁺CD25⁻CD45RB^{hi} T cells (Tnaive) or a non-colitis control of a 5:1 ratio of Tnaive cells with CD4⁺CD25⁺ T-regulatory cells (Treg) via intraperitoneal injection. Mice were weighed to monitor disease progression, and colons were evaluated for histologic injury at the indicated time point. (B) C57BL/6J mice were mock-infected with Luria broth (mock) or infected with 5.0×10^8 CFUs *Citrobacter rodentium* via oral gavage. Mice were weighed to monitor disease progression. Colons were harvested at day 14 and evaluated for histologic injury and enumeration of bacterial CFUs. Colon tissue was homogenized, serially diluted, and plated on MacConkey agar for enumeration of CFUs per gram of tissue. (C) CBA/J mice were infected via oral gavage with either 1.0×10^9 CFUs of either a STm T3SS mutant (*invA spiB*) or WT IR715 STm. Cecae were scored for histologic injury at the indicated time point. Stool was collected at the experimental endpoint, snap frozen, homogenized, serially diluted, and plated on MacConkey Agar for enumeration of bacterial CFUs per gram of stool. Error bars represent mean \pm standard error of the mean. Data analyzed via Student *t* test. *n* = 6–8 mice per group. ***P* < .01; ****P* < .001; *****P* < .0001.

Osteoclast Precursors Display Altered Surface Expression of Receptors Involved in Osteoclast Trafficking, Differentiation, and Function During DSS Colitis

Previous work has shown that the Cd11b^{-/lo}Ly6C^{hi} OCP population is highly osteoclastogenic, has distinct surface cytokine receptor expression patterns compared with other

myeloid cells, expresses receptors associated with osteoclast differentiation and function, and suppresses T cells.⁴⁷ Therefore, we next determined if intestinal inflammation alters the surface expression of receptors important in osteoclast trafficking, differentiation, and function in OCPs from mice with and without DSS colitis. We focused on early time points after DSS administration, given that we

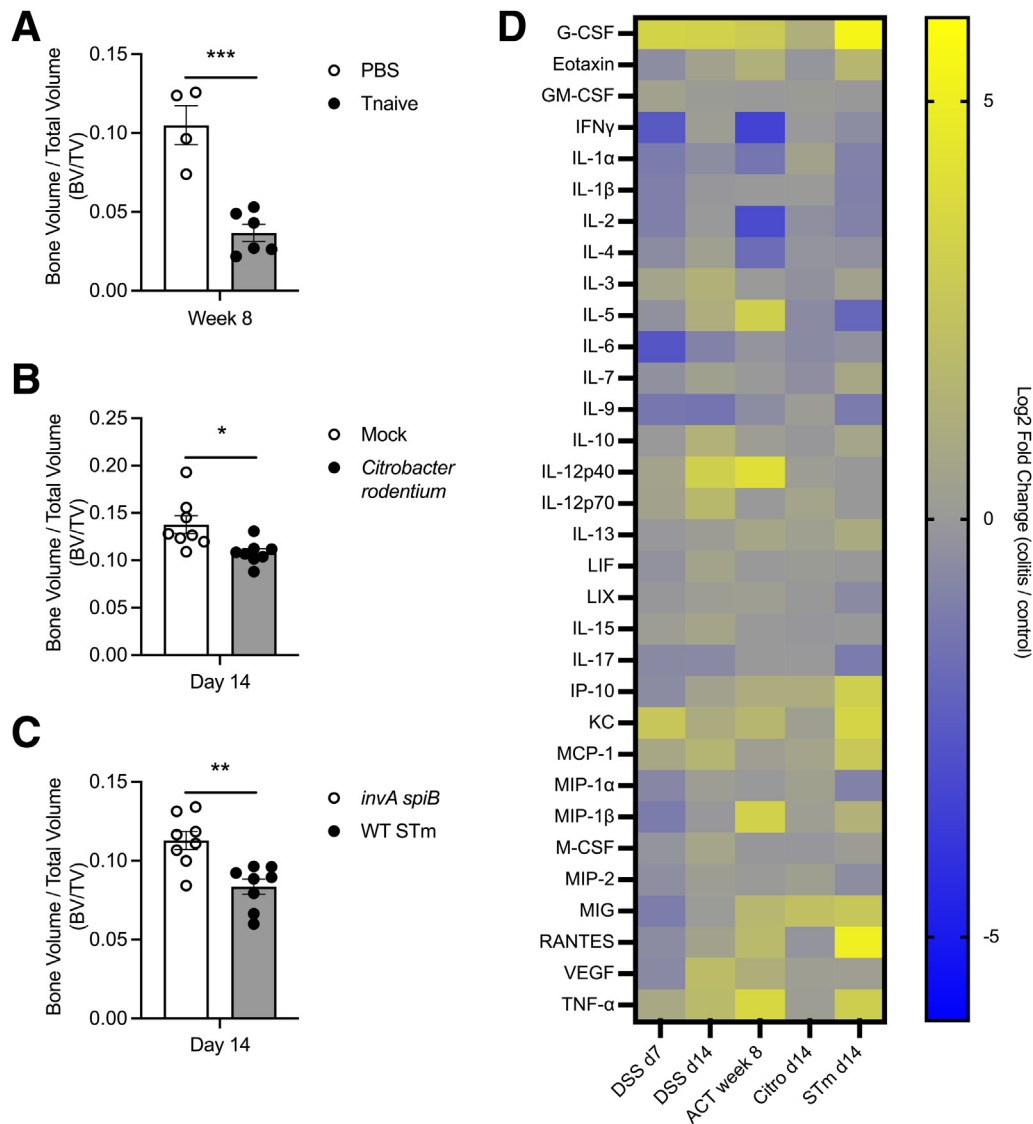


Figure 3. Multiple murine models of intestinal inflammation lead to bone loss and alter the bone marrow cytokine milieu. Mice were subjected to ACT, *Citrobacter rodentium* infection, or STm infection prior to harvest of femurs for micro CT analysis. (A) *Rag1*^{-/-} mice were administered 5.0×10^5 CD4⁺CD25⁻CD45RB^{hi} T cells (Tnaive) or PBS via intraperitoneal injection. (B) C57BL/6J mice were mock-infected with Luria broth (mock) or infected with 5.0×10^8 CFUs *Citrobacter rodentium* (Citro) via oral gavage. (C) CBA/J mice were infected with 1.0×10^9 CFUs of either WT STm strain IR715 (WT) or an *invA spiB* mutant via oral gavage. (D) Femurs from mice with or without intestinal inflammation were homogenized at the indicated time point and assessed for cytokine abundance via Luminex profiling. For DSS colitis, mice were administered 3% DSS for 7 days followed by 7 days of recovery with water. Heat map of cytokine abundance displayed as Log₂ fold change of mice with colitis relative to respective non-colitis controls. Error bars represent mean \pm standard error of the mean. Data analyzed via Student *t* test. *n* = 4–10 mice per group. **P* < .05; ***P* < .01; ****P* < .001.

observed an increase in osteoclast formation *in vivo* prior to trabecular bone loss (Figure 1, I–K). Because we observed significant increases in the abundance of MCP-1/CCL-2 in the femurs of mice treated with DSS prior to bone loss (Figure 4, C), we first examined the expression of the CCL-2 receptor, CCR2. We found that OCPs exhibited increased CCR2 expression (*P* < .0001) during DSS colitis compared with controls (Figure 6, B). Given that CCL-2/CCR2 signaling governs monocyte egress to sites of inflammation, such as the inflamed intestine, we next examined the expression of the tethering factor, CXCR4, which promotes retention of

Ly6C^{hi} monocytes within the bone marrow.⁴⁸ OCPs from mice with DSS colitis also demonstrated increased CXCR4 expression (*P* < .001) compared with control mice (Figure 6, C). Next, we measured surface expression of receptors that govern osteoclast differentiation. We detected a significant decrease in RANK expression (*P* < .01) but not CSF1R (*P* = .053) (Figure 6, D–E). Because we observed significant increases in several MDL-1-associated cytokines (eg, G-CSF, TNF- α , IL-23, and MCP-1/CCL2) in the femurs of mice with colitis, we evaluated MDL-1 expression on OCPs during DSS treatment (Figure 3, D and Figure 4).^{22–24,26} OCP

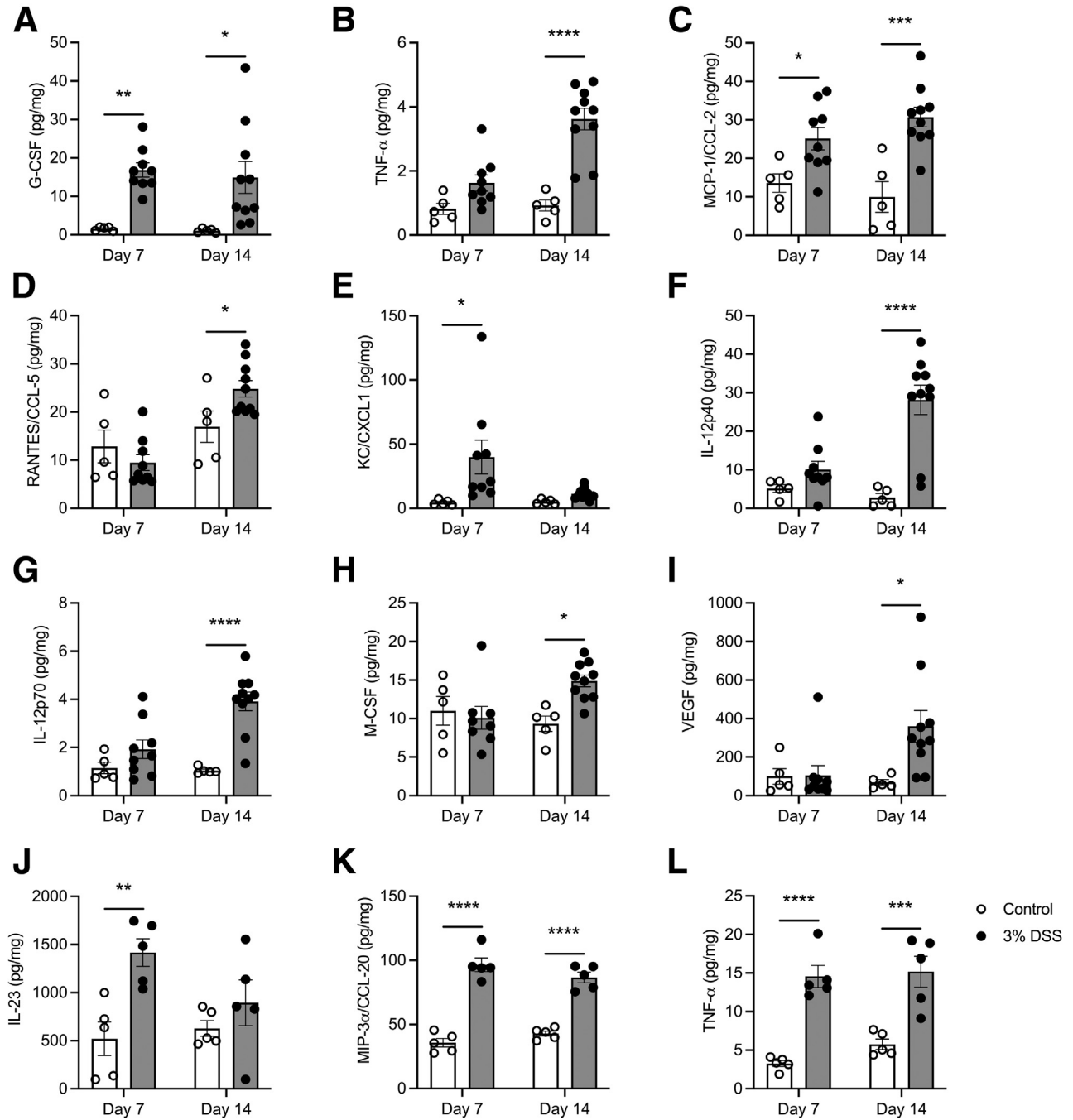


Figure 4. DSS colitis increases the abundance of MDL-1-associated cytokines. (A–I) Related to Figure 3, D. Mice were administered water (control, open circles) or 3% DSS (closed circles) for 7 days followed by 7 days of recovery with water. At the indicated time point, femurs from mice with or without intestinal inflammation were homogenized and assessed for cytokine abundance via Luminex profiling. Values were normalized to total protein as measured by a Pierce bicinchoninic acid (BCA) protein assay. Cytokines that were significantly elevated during colitis are shown. (A) G-CSF; (B) TNF- α ; (C) MCP-1/CCL-2; (D) RANTES/CCL-5; (E) KC/CXCL1; (F) IL-12p40; (G) IL-12p70; (H) M-CSF; (I) VEGF. (J–L) A separate cohort of mice were administered water (control, open circles) or 3% DSS (closed circles) for 7 days followed by 7 days of recovery with water and assessed for Th17-related cytokine abundance via Luminex profiling and normalized to total protein as measured by a Pierce BCA protein assay. Cytokines that were significantly elevated during colitis are shown. (J) IL-23; (K) MIP-3 α /CCL-20; and (L) TNF- α . Error bars represent mean \pm standard error of the mean. Data analyzed via 2-way ANOVA with Sidak multiple comparisons test. Post-hoc tests were only performed for significant ($P < .05$) ANOVAs. $n = 5$ –10 mice per group. * $P < .05$; ** $P < .01$; *** $P < .001$; **** $P < .0001$.

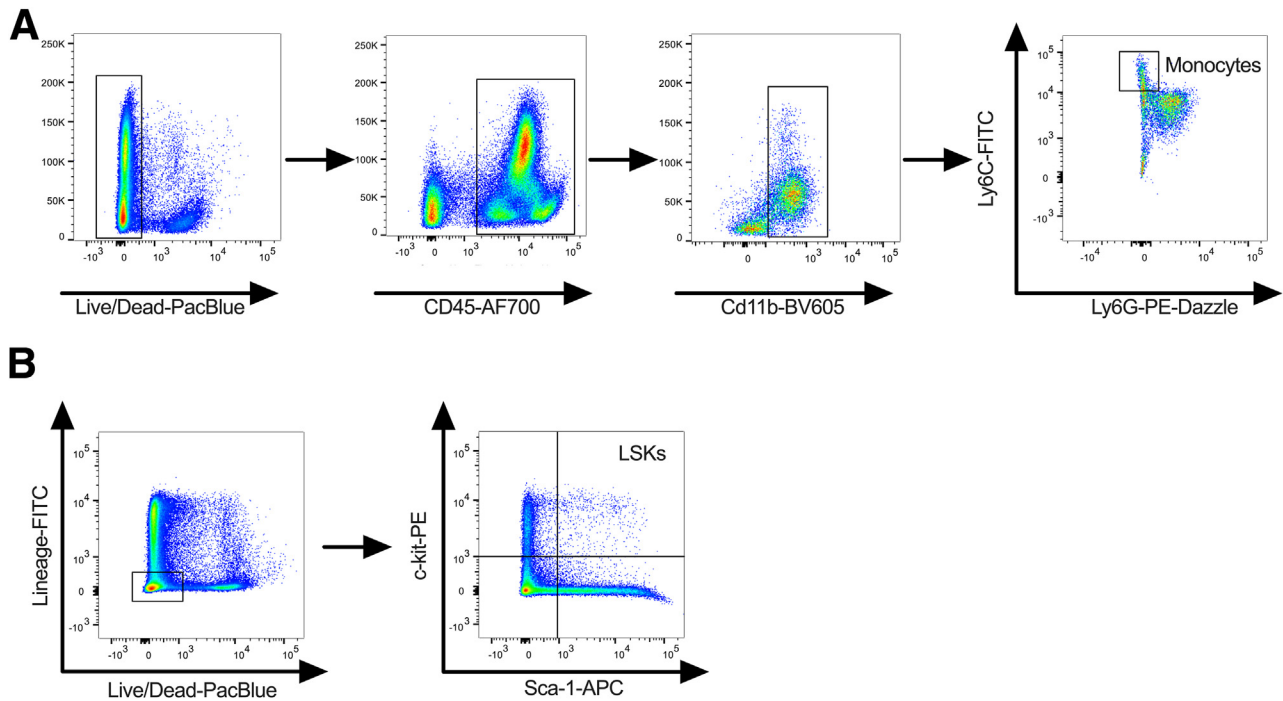


Figure 5. Gating strategy for monocytes and LSK populations. (A) Single cells were gated using successive gates including side scatter-area by forward scatter-area (SSC-A \times FSC-A), side scatter-height by area (SSC-H \times SSC-A), and forward scatter-height by area (FSC-H \times FSC-A) (not shown). Monocytes were then gated as live, CD45⁺Cd11b⁺Ly6C⁺Ly6G⁻ cells. (B) Single cells were gated as described above, after which cells were gated as live, LSK cells.

MDL-1 expression and the percentage of MDL-1⁺ OCPs were significantly increased ($P < .001$ and $P < .001$, respectively) during DSS colitis (Figure 6, F-H). To determine if the enhanced OCP MDL-1 expression was dependent on mature B or T cells, we administered 3% DSS to *Rag1*^{-/-}, which lack mature B and T lymphocytes. MDL-1 expression on OCPs and percentage of MDL-1⁺ OCPs was also significantly increased in *Rag1*^{-/-} mice given DSS ($P < .0001$ and $P < .001$) (Figure 6, I-K). To evaluate additional pro-osteoclastogenic co-receptors on OCPs during DSS colitis in WT mice, we measured surface expression of OSCAR, PIR-A/B, and TREM2. We noted similar increases in additional pro-osteoclastogenic co-receptors including OSCAR, PIR-A/B, and TREM2 (Figure 8, A-B). Increased OCP proliferation may represent one mechanism of increased osteoclast formation in vivo, as previous work has demonstrated that OCPs proliferate ex vivo in response to M-CSF.⁴⁷ To test the hypothesis that increased cellular proliferation may contribute to the increased osteoclast formation in vivo during intestinal inflammation, we evaluated intracellular Ki67 levels in OCPs from mice with or without DSS colitis. DSS treatment significantly increased Ki67 MFI (as determined by analysis of variance [ANOVA] $P < .05$) but not percent positive Ki67 OCPs (ANOVA $P = .09$) during DSS colitis (Figure 8, C-D). When correcting for multiple comparisons, however, no significant difference in Ki67 MFI at days 1 or 3 was observed following DSS treatment in comparison to control mice. These results suggest that OCPs may proliferate early in DSS colitis. Collectively, these data highlight that OCPs derived from mice subjected to

DSS-induced intestinal inflammation demonstrate changes in surface expression patterns of cytokine, chemokine, and osteoclast co-receptors associated with inflammation and enhanced osteoclastogenesis.

Anti-MDL-1 Antibody Treatment Blunts the Osteoclastogenic Potential of OCPs From Mice With Colitis and Ameliorates Colitis-associated Bone Loss

Given the increase in surface receptors associated with osteoclast differentiation and function, we next tested whether OCPs from mice with colitis are more prone to forming osteoclasts than those derived from healthy controls. To test this hypothesis, we sorted purified Cd11b^{-/lo} Ly6C^{hi} OCPs, Cd11b^{hi}Ly6C⁺ monocytes, or Cd11b⁻Ly6C⁻ double-negative cells from the bone marrow of mice with or without DSS colitis and cultured these cells in the presence of exogenous M-CSF and RANKL. We observed that DSS treatment increased the ex vivo osteoclastogenic potential of purified monocytes, OCPs, and unsorted whole bone marrow (input) (Figure 9, A). OCPs displayed the highest osteoclastogenic potential (Figure 9, A). Because the surface expression of the pro-osteoclastogenic coreceptor MDL-1 was increased on DSS-derived OCPs, we assessed whether ex vivo anti-MDL-1 antibody treatment could blunt the enhanced osteoclast formation potential of these cells. In comparison to isotype control, treatment with anti-MDL-1 antibody abrogated the increased osteoclast formation of OCPs isolated from DSS-treated mice ($P < .0001$) (Figure 9, A).

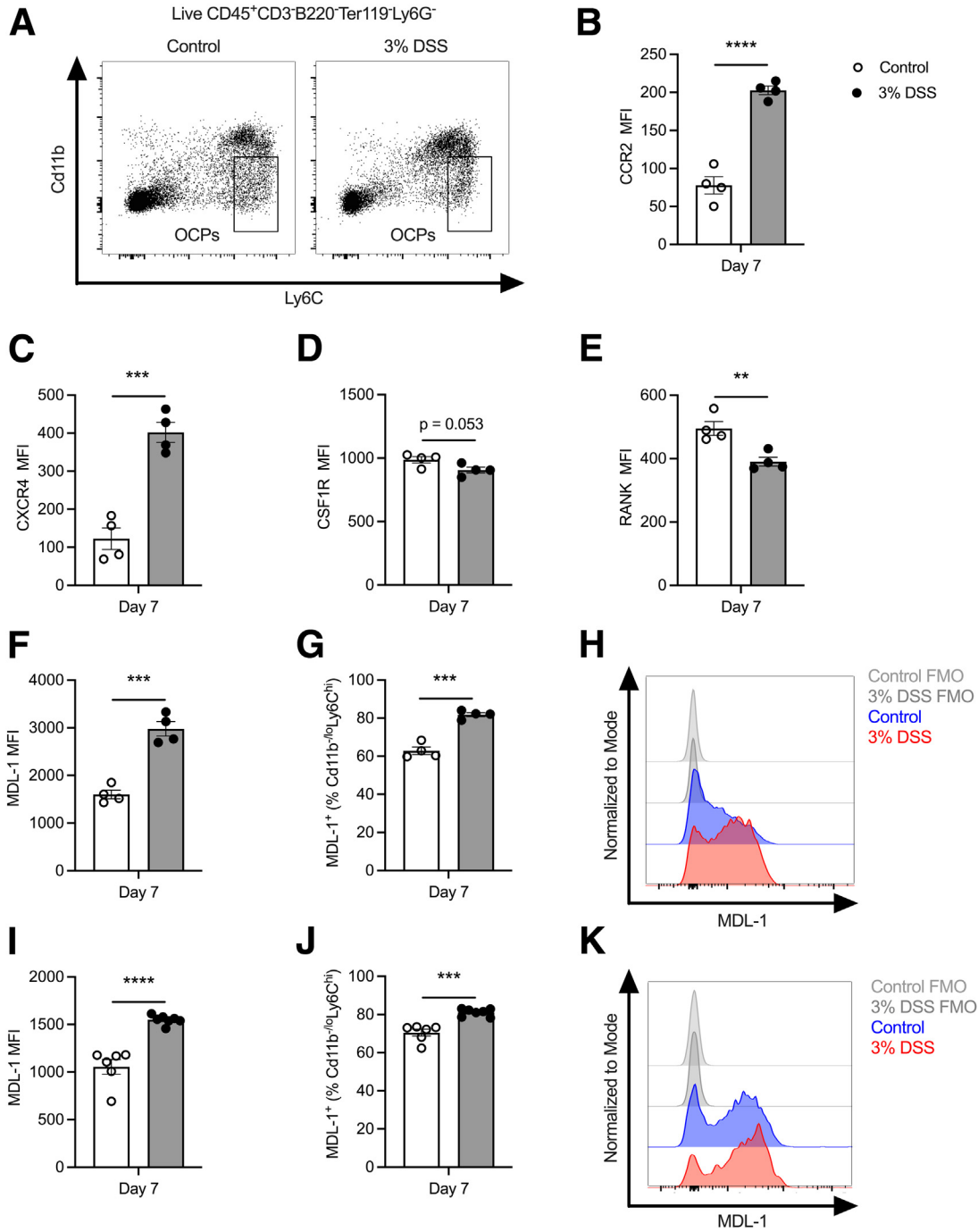


Figure 6. OCPs isolated from mice with DSS colitis demonstrate altered expression of receptors involved in osteoclast differentiation and function. C57BL/6J (A–H) or *Rag1*^{-/-} (I–K) mice were administered 3% DSS or water (control) for 7 days, after which bone marrow was processed for flow cytometry. (A) Gating strategy for Cd11b^{lo}Ly6C^{hi} OCPs. (B–F) Mean fluorescence intensity (MFI) of surface markers related to osteoclast differentiation and function from C57BL/6J mice with (filled circles) or without (open circles) colitis including CCR2 (B) CXCR4 (C) colony stimulating factor 1 receptor (CSF1R) (D) receptor activator of nuclear factor kappa-B (RANK) (E) and MDL-1 (F). (G) Percent positive MDL-1 OCPs. (H) Representative histogram of MDL-1 distribution among OCPs. (I) OCP MDL-1 MFI, percent MDL-1⁺ OCPs (J) and representative histogram of MDL-1 staining (K) on OCPs derived from *Rag1*^{-/-} mice with or without colitis. FMO, Fluorescence minus one control. Error bars represent mean ± standard error of the mean. Data analyzed via Student *t* test. n = 4–7 mice per group. ***P* < .05; ****P* < .001; *****P* < .0001.

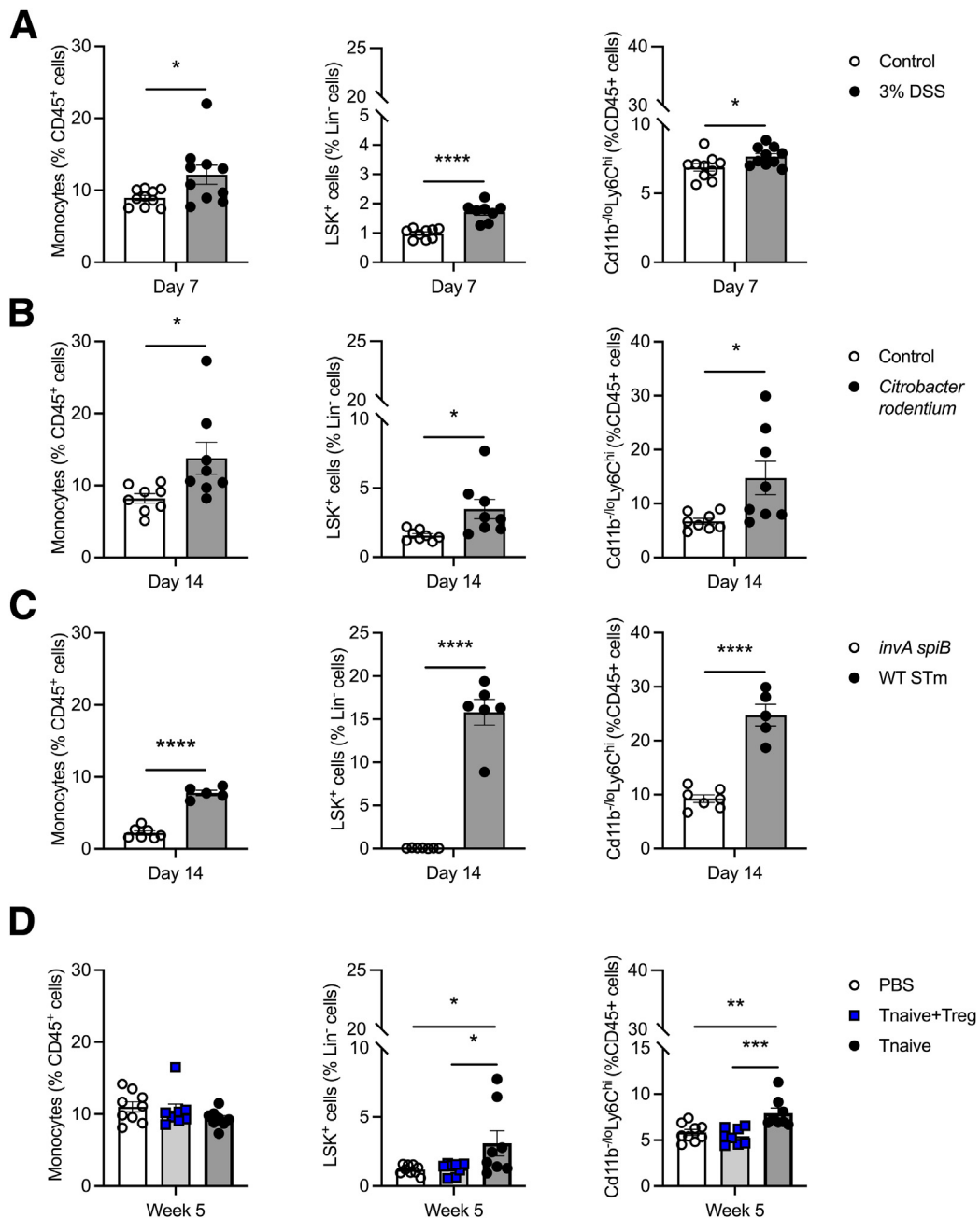


Figure 7. Multiple murine models of colitis alter the relative abundance of OCPs within the bone marrow. (A) C57BL/6J mice were administered either water (control, open circles) or 3% DSS (closed circles) for 7 days. (B) C57BL/6J Mice were mock-infected (mock) with Luria broth or infected with *Citrobacter rodentium* via oral gavage. (C) CBA/J mice were infected via oral gavage with either a STm mutant (*invA spiB*) or WT IR715 STm. (D) *Rag1*^{-/-} mice were injected with either 5.0×10^5 CD4⁺CD25⁻CD45RB^{hi} T cells (Tnaive), a non-colitis control of a 5:1 ratio of Tnaive cells with CD4⁺CD25⁺ T-regulatory cells (Treg), or PBS via intraperitoneal injection. Tibias and femurs were harvested at the indicated time points, and bone marrow was collected for flow cytometry. Bone marrow cells were stained with a panel of antibodies to identify monocytes by lineage (CD45⁺Ter119⁻CD3⁻B220⁻Cd11b⁺LyC⁺Ly6G⁻), LSK cells (Lin⁻sca-1⁺c-kit⁺), and Cd11b^{-/-}Ly6C^{hi} OCPs (CD45⁺Ter119⁻CD3⁻B220⁻Ly6G⁻Cd11b^{-/-}Ly6C^{hi}). Error bars represent mean \pm standard error of the mean. Data analyzed via Student *t* test (A–C) or 1-way ANOVA with Sidák multiple comparisons test (D). Post-hoc tests were only performed for significant ($P < .05$) ANOVAs. $n = 5$ –10 mice per group. * $P < .05$; ** $P < .01$; *** $P < .001$; **** $P < .0001$.

Because anti-MDL-1 antibody could blunt ex vivo osteoclastogenesis of OCPs harvested from mice with colitis, we tested if this antibody could reduce bone loss in vivo in mice with experimental colitis. We first determined if anti-

MDL-1 impacted baseline trabecular bone architecture in healthy control mice. No differences were observed in weight or trabecular bone parameters in mice receiving a single injection of anti-MDL-1 compared with IgG isotype

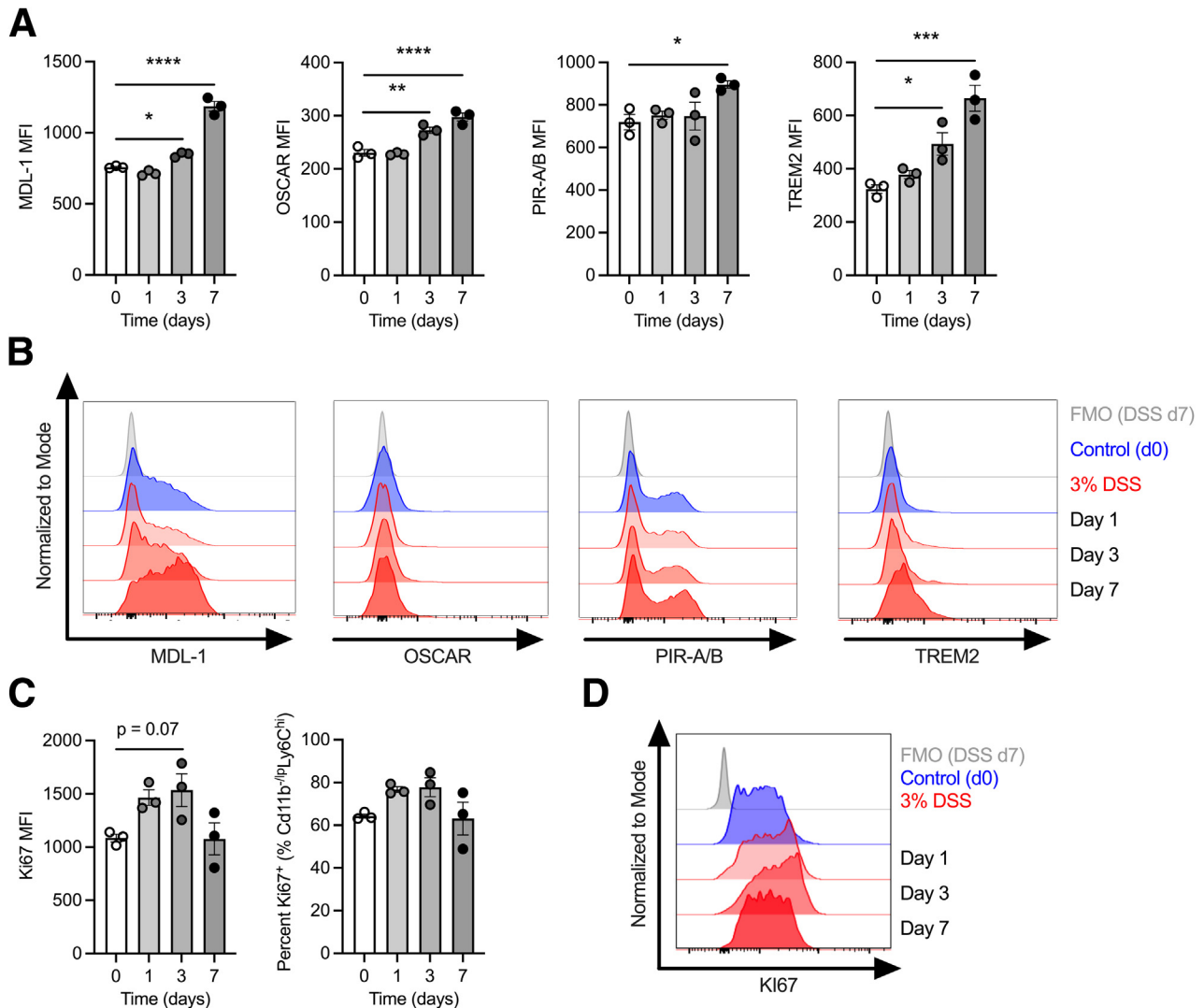


Figure 8. DSS-induced colitis alters osteoclast co-receptor expression within the bone marrow. C57BL/6J mice were administered 3% DSS for 0, 1, 3, or 7 days. Bone marrow was isolated from the long bones of mice with or without colitis on the indicated day and processed for flow cytometry. Cd11b^{-lo}Ly6C^{hi} OCPs were stained for either MDL-1, OSCAR, PIR-A/B, TREM2, or intracellular Ki67. (A) Mean fluorescence intensity (MFI) of osteoclast co-receptors at the indicated time point following DSS administration; (B) Representative histogram of osteoclast co-receptor staining. (C) MFI and percent positive of Cd11b^{-lo}Ly6C^{hi} OCP intracellular Ki67 staining at the indicated time point following 3% DSS administration; (D) Representative histogram of Ki67 staining. Error bars represent mean \pm standard error of the mean. Data analyzed via 1-way ANOVA with Sidák multiple comparisons test. Post-hoc tests were only performed for significant ($P < .05$) ANOVAs. $n = 3$ mice per group. * $P < .05$; ** $P < .01$; *** $P < .001$; **** $P < .0001$.

control (Figure 9, C–D). We next evaluated whether in vivo anti-MDL-1 antibody treatment can reduce bone loss during DSS colitis. Because we observed an increase in OCP MDL-1 expression as early as day 3 following DSS administration (Figure 8, A–B), we administered monoclonal anti-MDL-1 antibody or IgG isotype control treatment to DSS-treated mice at day 3 following colitis induction (Figure 9, B). Anti-MDL-1 treated mice demonstrated no significant differences in histologic injury and demonstrated similar weight changes compared with isotype IgG control treated mice during colitis (Figure 9, C and E). Mice treated with anti-MDL-1 demonstrated a 27% increase in BV/TV compared with mice treated with isotype control ($P < .05$),

which was associated with significantly increased trabecular thickness ($P < .05$) (Figure 9, F–K).

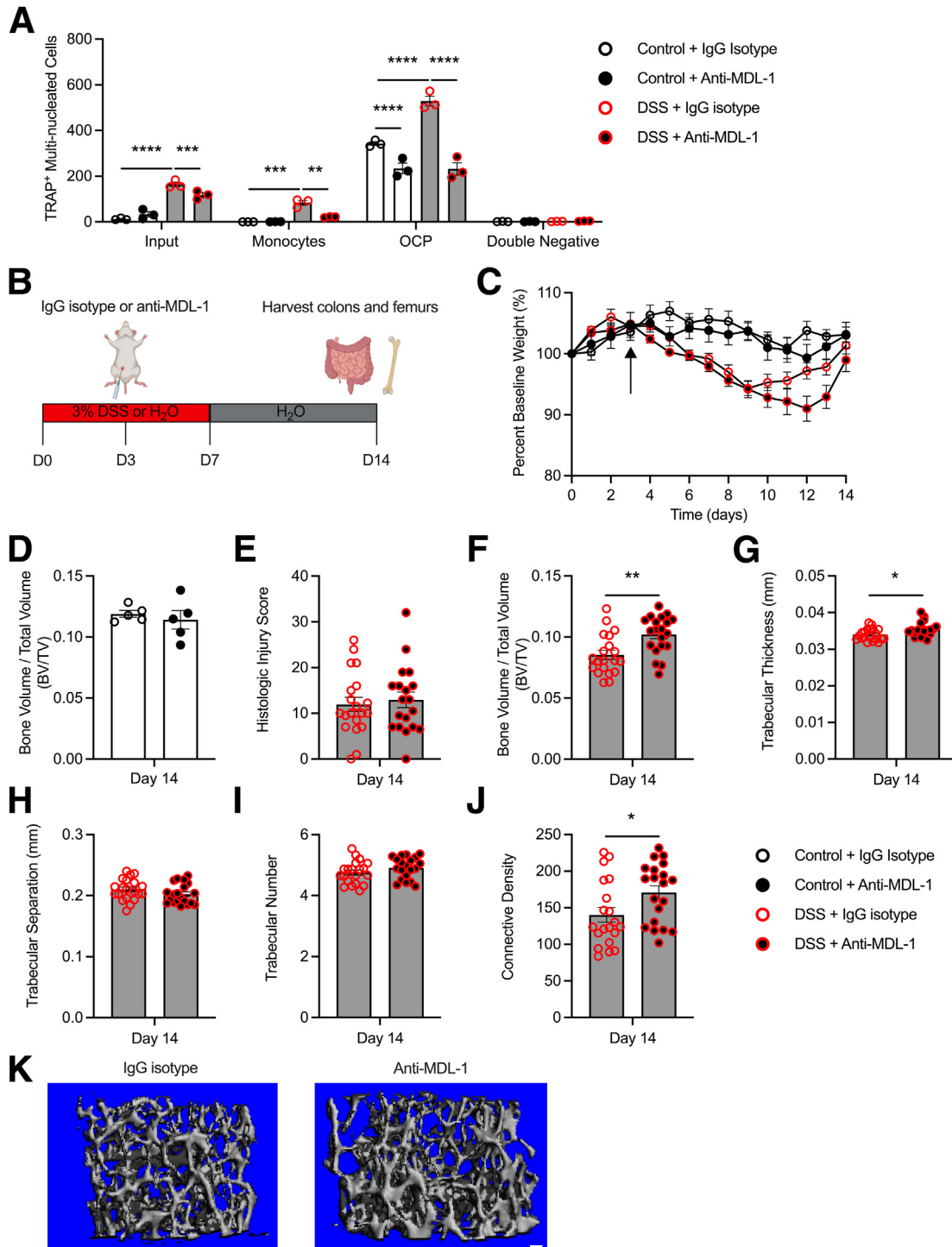
Discussion

The data from this study demonstrate that multiple murine models of IBD result in concomitant bone loss. Significant increases in the relative abundance of a highly osteoclastogenic pre-osteoclast population were observed across 4 models of intestinal inflammation. Furthermore, this study reveals that during DSS colitis, OCPs demonstrate altered cytokine-, chemokine-, and osteoclast-associated receptors, as compared with OCPs from control mice. The

changes to OCP surface receptor expression also occurred in *Rag1*^{-/-} mice, suggesting that both the expansion and alteration of OCPs during DSS colitis are not solely dependent on interactions with inflammatory T cells, B cells, or their cytokines. OCPs from mice with colitis demonstrate increased osteoclast formation *ex vivo* when compared with OCPs derived from control mice, and this enhanced osteoclastogenesis is blunted by anti-MDL-1 antibody treatment. *In vivo*, a single dose of anti-MDL-1 antibody reduced bone

loss during DSS colitis. Collectively, these data reveal that OCPs derived from mice with intestinal inflammation have enhanced osteoclastogenesis *ex vivo*, that this increased osteoclast formation is associated with increased MDL-1 surface expression on OCPs, and that *in vivo* anti-MDL-1 antibody treatment can ameliorate bone loss during DSS colitis.

We observed marked increases in cytokines and chemokines capable of inducing MDL-1 expression, most



notably G-CSF, in the femurs of mice subjected to models of colitis. This increase in MDL-1-associated cytokines corresponded with a robust increase in expression of MDL-1 on OCPs. Recent evidence has linked MDL-1 with IBD pathogenesis, as MDL-1⁺ TNF- α ⁺ monocytes have been found to be significantly increased in the lamina propria of patients with IBD.⁴⁹ Single-cell and bulk-RNA sequencing studies have additionally highlighted increases in MDL-1 (*CLEC5A*) expression in inflamed intestinal tissue compared with control-matched non-inflamed tissue.^{50,51} Although human and murine correlates of bone marrow OCPs are poorly defined, bulk-RNA sequencing from human PBMCs has also revealed increases in *CLEC5A* expression in patients with IBD compared with age and sex-matched controls.⁵² Furthermore, *CLEC5A* expression has been identified by single-cell RNA-seq as a gene associated with an inflammatory monocyte cytokine module within the Risk Stratification and Identification of Immunogenetic and Microbial Markers of Rapid Disease Progression in Children with Crohn's Disease (RISK) study.⁵³

In addition to mediating inflammatory responses, MDL-1 plays an important role in osteoclast formation and triggers osteoclastogenesis by forming a trimolecular complex with DAP-10 and DAP-12.⁵⁴ Previous work has demonstrated that OCPs express MDL-1, but studies to date have not examined how MDL-1 or other co-receptors involved in osteoclast differentiation and function change during intestinal inflammation.⁴⁷ MDL-1 has been reported to form a complex with the IL-23R in human monocytes, and IL-23 treatment of human monocytes leads to both osteoclast differentiation and increased MDL-1 expression.²⁴ Although we did not evaluate OCPs from human bone marrow, these prior studies utilizing human monocytes suggest that MDL-1⁺ OCPs could potentiate IBD-associated bone loss in humans. Taken together, these observations suggest a mechanism whereby specific inflammatory cytokines associated with IBD pathogenesis impact the expression of osteoclast coreceptors on OCPs to drive osteoclastogenesis and bone loss.

In addition to increased MDL-1 expression, data from this study also demonstrate that OCPs exhibit increased expression of surface molecules important in osteoclast trafficking (CCR2 and CXCR4) during colitis. Elevated CCR2 may reflect that OCPs during colitis are primed to exit the bone marrow environment and traffic to the inflamed intestine. However, OCPs expressed higher levels of the tethering factor, CXCR4, indicating that these cells might instead be more tightly tethered to the bone marrow environment or contribute to replenishing monocyte pools.⁴⁸ Although G-CSF, which was significantly elevated in the bone across all models of colitis, has been shown to reduce CXCR4 expression in Gr-1⁺ myeloid cells as a mechanism of mobilization, it conversely increases CXCR4 expression on HSCs.^{55,56} OCPs were originally reported to retain clonogenic potential as measured by colony formation.⁴⁷ Therefore, G-CSF may induce CXCR4 expression in OCPs in a manner similar to that previously reported for HSCs. Future studies are needed to investigate how intestinal inflammation alters the tethering and mobilization properties of OCPs.

Although an expansion of OCPs represents one potential mechanism for increased osteoclastogenesis during DSS colitis, this study also demonstrates that colitis alters expression of surface receptors that directly govern osteoclast differentiation and function (RANK, CSF1R, MDL-1, OSCAR, TREM2, and PIR-A/B). OCPs from mice with DSS colitis demonstrated a subtle but statistically significant reduction in RANK expression. The functional consequences of reduced RANK are unclear, although DSS-derived OCPs maintained the ability to form robust osteoclasts ex vivo in response to treatment with respective ligands RANKL and M-CSF. TNF- α , which was increased in the femur homogenates across multiple murine models of colitis, has previously been shown to induce both OSCAR and PIR-A in addition to MDL-1.^{57,58} Accordingly, in addition to an increase in abundance of OCPs, enhanced sensitivity to pro-osteoclastogenic signals is likely a complementary mechanism that contributes to increased osteoclastogenesis and bone loss during DSS colitis.

Figure 9. (See previous page). Anti-MDL-1 antibody treatment blunts ex vivo osteoclastogenesis and protects against colitis-associated bone loss in vivo. (A) C57BL/6J mice were administered either 3% DSS or water (control) for 7 days. Bone marrow was isolated on day 7 following DSS treatment from the long bones of mice with or without colitis and processed for FACS. Unsorted whole bone marrow (input), Cd11b⁺Ly6C⁺ monocytes, Cd11b^{lo}Ly6C^{hi} OCPs, or Cd11b⁻Ly6C⁻ (double negative) cells were seeded at either 5.0×10^4 (input) or 1.0×10^4 cells/mL (sorted), differentiated for 4 days with 5% v/v CMG14-12 supernatant and 35 ng/mL RANKL in the presence or absence of 10 μ g/mL IgG isotype control or anti-MDL-1 antibody. After 4 days, cells were stained for TRAP, and multi-nucleated TRAP⁺ cells were manually enumerated. (B) Experimental design for in vivo anti-MDL-1 antibody treatment. C57BL/6J mice were administered 3% DSS or water (control) for 7 days, after which time mice were switched to water. At day 3 following DSS administration, mice received a single dose of 50 μ g of either IgG isotype control or anti-MDL-1 antibody via intraperitoneal injection. Colons and femurs were harvested at day 14 following DSS administration. Created with BioRender.com. (C) Percent baseline weight of DSS-treated mice receiving either isotype control or anti-MDL-1 antibody. Arrow indicates time of IgG isotype or anti-MDL-1 antibody. (D) Micro CT analysis of formalin-fixed femurs from control mice receiving either isotype or anti-MDL-1 antibody for trabecular BV/TV. (E) Histologic injury score of H&E colons from DSS-treated mice receiving either isotype control or anti-MDL-1 antibody. (F–K) Micro CT analysis of formalin-fixed femurs from DSS-treated mice receiving either isotype or anti-MDL-1 antibody for BV/TV (F) trabecular thickness (G) trabecular separation (H) trabecular number (I) connective density (J) and representative 3-dimensional reconstruction of trabecular bone from mice treated with either isotype or anti-MDL-1 antibody (K). Scale bar = 100 μ m. Error bars represent mean \pm standard error of the mean. Data analyzed via 2-way ANOVA with Sidak multiple comparisons test for comparisons within each sorted population (A) or Student *t* test (D–J). Post-hoc tests were only performed for significant ($P < .05$) ANOVAs. $n = 3$ independent cultures (A) 5 mice (controls, C–D), or 20 mice per group (DSS; C, E–J). * $P < .05$; ** $P < .01$; *** $P < .001$; **** $P < .0001$.

In this study, DSS colitis led to an increase in osteoclast formation in purified monocyte and OCP populations *ex vivo*. OCPs from DSS-treated mice displayed similar Ki67 levels as controls at day 7 following DSS administration. Therefore, cell cycling prior to exogenous M-CSF and RANKL administration likely does not explain the differences in osteoclast formation *ex vivo*. However, Ki67 MFI significantly increased during DSS administration, and this was most pronounced at early time points following DSS treatment. But these data did not reach statistical significance following correction for multiple comparisons, and therefore, additional experiments are necessary to test if increased cell cycling at days 1 and 3 following DSS colitis contributes to the expansion of OCPs.

There are some limitations of this work that will drive future studies. Because the goal of this study was to evaluate how intestinal inflammation alters osteoclasts and their precursors, we did not examine other important contributors to bone loss during IBD, such as nutrition and alterations to osteoblast biology. Therefore, these data do not exclude additional complementary mechanisms of IBD-associated bone loss that occur through nutritional deficits or altered osteoblast function, which have been highlighted in previous studies.^{31–33,59–62} We did observe bone loss in colitis models that were not associated with significant weight loss, which is consistent with previous reports and may point to mechanisms that are independent of nutritional status.³³ Future studies should address the relative contributions of OCPs, nutritional status, and osteoblast function in contributing to bone loss during intestinal inflammation. Although several important osteoclast precursors were found to expand during colitis, this study did not evaluate alternative cell lineages (eg, dendritic cells) capable of osteoclastogenesis, and therefore cannot exclude their contribution to bone loss during intestinal inflammation. Anti-MDL-1 antibody treatment reduced osteoclast formation in OCPs isolated from DSS-treated mice *ex vivo*. Moreover, treating mice with a single dose of anti-MDL-1 antibody decreased bone loss *in vivo* during DSS colitis and did not significantly impact the severity of colitis. The ideal IBD therapeutic would not only target bone loss, but also treat the underlying intestinal inflammation to prevent inflammatory bone loss from occurring. However, targeting the MDL-1 axis to ameliorate bone loss during IBD may still be clinically efficacious in those patients who experience bone loss or non-healing fractures despite maximal intestinal-targeted therapy. Future studies should evaluate if MDL-1 blockade is effective in reducing IBD-associated bone loss when combined with standard of care therapy, such as anti-cytokine monoclonal antibodies. Future investigations should also test if anti-MDL-1 antibody treatment ameliorates bone loss in other models of intestinal inflammation. Furthermore, the generation of cell-specific knockouts of MDL-1 will also help to clarify cell-intrinsic versus cell-extrinsic roles of MDL-1 in colitis-associated bone loss. Previous work has demonstrated that blockade of MDL-1 prevents inflammatory-mediated bone loss in a murine model of inflammatory arthritis without impacting baseline bone formation, and we similarly did not observe

an impact of anti-MDL-1 treatment on baseline bone parameters.²³ Endogenous ligands for many osteoclast co-receptors, including MDL-1, remain poorly described. Deciphering the precise ligands that MDL-1 binds and understanding how monoclonal antibodies may disrupt these interactions remains an important area for future research. Ligands for DAP-12 associated receptors, such as MDL-1, are thought to be expressed on the same myeloid OCP populations.¹⁴ Additional work is also needed to evaluate MDL-1 expression on OCPs derived from humans with active vs quiescent IBD. Overall, this study demonstrates that intestinal inflammation significantly alters pre-osteoclast populations and implicates the osteoclast co-receptor, MDL-1, as a key mediator of bone loss during colitis.

Materials and Methods

Ethics Statement

All animal experiments were reviewed and approved by the Institutional Animal Care and Use Committee at Vanderbilt University Medical Center on the animal protocol M1600147-01. All experiments were conducted in accordance with National Institutes of Health guidelines, the Animal Welfare Act, and United States Federal Law, and performed with institutional biosafety committee approval. Mice were euthanized by CO₂ asphyxiation with secondary confirmation by cervical dislocation and observation of heart rate and breathing. All authors had access to the study data and reviewed and approved the final manuscript.

Animal Use

Male and female 7- to 9-week-old C57BL/6J (Stock # 000664), CBA/J (Stock # 000656), and *Rag1*^{-/-} (Stock # 002216) mice were purchased through The Jackson Laboratory and maintained in our colony for 1 week prior to experimentation. C57BL/6J, CBA/J, and *Rag1*^{-/-} mice were bred homozygously. C57BL/6J and CBA/J mice were maintained in specific pathogen-free conditions. *Rag1*^{-/-} mice were maintained in sterile conditions with autoclaved food and bedding prior to adoptive T cell transfer, after which they were switched to specific pathogen-free conditions.

Mouse Models of Colitis

For experiments involving DSS colitis, 3% DSS (TdB Labs) was administered *ad libitum* in the sterile drinking water of 7-week-old male or female WT or *Rag1*^{-/-} mice for 1 week, after which time mice were switched back to sterile drinking water. Mice were euthanized at days 1, 3, 7, or 14 following the initiation of DSS treatment. Where indicated, mice were treated with 50 µg of either anti-MDL-1 (R&D, clone 226402) or IgG2a isotype control (R&D clone 54447) at day 3 following DSS-treatment or in control mice not treated with DSS. Mice were monitored for signs of clinical disease and weighed daily. For experiments involving adoptive T cell transfer, colitis was induced in male or female C57BL/6J *Rag1*^{-/-} mice by adoptive transfer of sorted CD4⁺CD25⁻CD45RB^{hi} cells. CD4⁺ T cells were isolated from the splenocytes of WT 8–12-week-old sex-matched C57BL/6J mice using negative selection magnetic enrichment (Stem

Cell Technologies) per the manufacturer's instructions. Enriched CD4⁺ T cells were stained with a surface staining cocktail including CD4-APC-Cy7 (Biolegend, clone GK1.5), CD25-APC (Biolegend, clone PC6.1), and CD45RB-BV711 (BD Optibuild, clone 16A), as well as a live/dead stain (eBioscience Fixable Viability Dye eFluor 506). Live CD4⁺CD25⁻CD45RB^{hi} (Tnaive) and live CD4⁺CD25⁺CD45RB⁻ (Treg) cells were sorted by fluorescent automated cell sorting (FACS) using either 4- or 5-laser FACS Aria III systems. Naïve T cells were gated to include the CD4⁺ T cells demonstrating the top 30% to 40% expression of CD45RB. 5.0×10^5 Tnaive or a combination of 5.0×10^5 Tnaive and 1.0×10^5 Treg cells (non-colitis control) were adoptively transferred into sex-matched 8-10-week-old C57BL/6J *Rag1*^{-/-} recipient mice by intraperitoneal injection. Post-sort viability of Tnaive and Treg cells was routinely observed to be >85%. Mice were weighed weekly, monitored for disease progression, and euthanized at weeks 5 or 8 post-transfer. For experiments involving *Citrobacter rodentium* colitis, infection was achieved as previously described.^{63,64} Briefly, male C57BL/6J mice were infected by oral gavage with 5.0×10^8 colony-forming units (CFUs) of *C. rodentium* or mock-infected with Luria broth. Mice were weighed and monitored for disease progression. Colon tissue was homogenized, serially diluted, and plated on MacConkey Agar for enumeration of bacterial CFUs per gram of stool. For experiments involving STm, CBA/J mice were infected as previously described.⁶⁵ 8-week-old CBA/J female mice were infected via oral gavage with 1.0×10^9 CFUs of STm strain IR715 or an isogenic mutant lacking functional T3SS1 and T3SS2 ($\Delta invA::tetRA \Delta spiB::KSAC$, herein referred to as *invA spiB*). Mice were weighed and monitored for disease progression. Stool was collected throughout the course of infection and at the experimental endpoint, snap frozen, homogenized, serially diluted, and plated on MacConkey agar for enumeration of bacterial CFUs per gram of stool.

Colitis Scoring

Colons from mice with or without colitis were harvested at the indicated experimental time point, swiss-rolled, fixed in 10% neutral buffered formalin for 24 hours, and subsequently processed for paraffin embedding, sectioning, and staining with hematoxylin and eosin (H&E). For STm infections, ceca were harvested at the indicated time point and processed as stated above for colons. H&E-stained colon sections were scored in a blinded manner by a gastrointestinal pathologist (M.B.P.) using previously published scoring criteria for DSS colitis,⁶⁶ adoptive T cell transfer colitis,⁶⁷ and *C. rodentium* induced colitis.^{63,64} H&E-stained cecal sections were scored in a blinded manner by a veterinary pathologist (M.X.B.) using previously published scoring criteria.⁶⁵

Micro CT of Trabecular Bone

Femurs were harvested at the indicated time point and fixed with 10% neutral buffered formalin for 48 hours at 4 °C and then placed in 70% ethanol. Trabecular bone was

analyzed using a μ CT40 (Scanco Medical, AG Bassersdorf, Switzerland) and Scanco software. Images were acquired at 55 kVp and 145 mA with an isotropic voxel size of 12 μ m and an integration time of 250 ms with 1000 projections collected per 360° rotation. Images were reconstructed, filtered (sigma = 0.8; support = 1.0), and thresholded at 200 mg HA/ccm. Trabecular bone at the distal femur was manually contoured every 10 slices starting 30 slices proximal to the growth plate and advancing proximally for 100 slices such that trabeculae were included, and cortical bone was excluded in accordance with American Society for Bone and Mineral Research (ASBMR) guidelines.⁶⁸ Sections between manual contours were automatically contoured.

Bone Histology and Histomorphometry

Following micro CT imaging, femurs were decalcified for 3 days in 20% EDTA (pH 7.4) at 4 °C. Samples were then dehydrated, embedded in paraffin blocks, and sectioned longitudinally at 4 μ m thickness through the medullary cavity with a Leica RM2255 microtome. Tissue sections were mounted onto Leica Superfrost glass slides and then stained with TRAP stain with hematoxylin counterstain. Bioquant software (Nashville, TN) was used to perform quantitative histomorphometry (osteoclast number, osteoclast surface, and bone perimeter) in accordance with ASBMR guidelines using 10 \times images generated from a Cytation 5 imaging system (Biotek).⁶⁹

Flow Cytometry and Cell Sorting

Bone marrow from murine femurs and tibias was flushed with cold alpha-minimal essential media. Red blood cells were lysed for 5 minutes with ammonium chloride potassium lysing buffer, pelleted, resuspended in phosphate buffered saline (PBS), and passed through a 70- μ m filter. Single-cell suspensions were washed with PBS, enumerated, and 1 million bone marrow cells per sample were pelleted in PBS prior to live/dead staining per the manufacturer's protocol (Zombie Violet, Biolegend). Cells were then washed with FACS buffer (PBS containing 3% fetal bovine serum and 0.1% sodium azide). Non-specific antibody staining was blocked with anti-CD16/32 (Biolegend, clone 93) for 15 minutes at room temperature. Single-cell bone marrow suspensions were stained with a cocktail of surface-staining antibodies to identify specific myeloid populations. Unless otherwise indicated, all antibodies were purchased from Biolegend. For OCPs and monocytes, the following anti-mouse antibodies were used: Anti-CD45-AlexaFluor700 (clone 30-F11), anti-Cd11b-BV605 (clone M1/70), anti-Ly6G-PE or anti-Ly6G-PE-Dazzle (clone 1A8), anti-Ly6C-FITC (clone HK1.4), anti-TER119-Pacific Blue (clone TER-119), anti-B220-Pacific Blue (clone RA3-6B2), anti-CD3-Pacific Blue (clone 145-2C11). For LSK cells, the following antibodies were used: Anti-mouse lineage cocktail-FITC (clones 145-2C11, RB6-8C5, RA3-6B2, Ter-119, M1/70), anti-Sca-1-APC (clone D7), and anti-c-kit-PE (clone QA17A09). Additional surface markers were evaluated on monocytes and OCPs by staining with anti-CXCR4-BV-711 (clone L276F12), anti-MDL-1-APC (Miltenyi, clone REA582), anti-CX₃CR1-APC (clone SA011F11), anti-CCR2-

APC/Fire-750 (clone SA203G11), anti-RANK-PE (clone R12-31), and anti-CSF1R-PerCP/Cy5.5 (clone AFS98). Osteoclast co-receptors antibodies specific for OSCAR (Novus Biologicals, clone 5B8), PIR-A/B (clone 6C1), and TREM2 (R&D, clone 237920) were conjugated to APC using the APC conjugation kit – lightning link (Abcam) per the manufacturer's instructions. Surface staining was accomplished by incubating single cell suspensions with a given antibody cocktail at 4 °C for 30 minutes. For intracellular staining, cells were fixed and permeabilized overnight at 4 °C using the Foxp3 / transcription factor staining buffer set (eBioscience) per manufacturer's instructions followed by intracellular staining for Ki67-APC (clone 16A8). Cells were washed twice in FACS buffer and fixed in PBS with 2% paraformaldehyde and analyzed using a 3- or 4-Laser Fortessa analytical flow-cytometer. Single cells were gated using successive gates including side scatter-area by forward scatter-area (SSC-A × FSC-A), side scatter-height by area (SSC-H × SSC-A), and forward scatter-height by area (FSC-H × FSC-A). Gating for the indicated populations was done as described in Figure 5 and Figure 6, A. For cell sorting, single-cell bone marrow suspensions were obtained as described above, live-dead stained, and blocked as described above. Cells were stained with Anti-CD45-AlexaFluor700 (clone 30-F11), anti-Cd11b-BV605 (clone M1/70), anti-Ly6G-PE (clone 1A8), anti-Ly6C-FITC (clone HK1.4), anti-TER119-Pacific Blue (clone TER-119), anti-B220-Pacific Blue (clone RA3-6B2), and anti-CD3-Pacific Blue (clone 145-2C11). Monocytes (live CD3⁻B220⁻Ter119⁻Ly6G⁻CD45⁺Cd11b⁺Ly6C⁺) OCPs (live CD3⁻B220⁻Ter119⁻Ly6G⁻CD45⁺Cd11b^{hi}Ly6C^{hi}) or Cd11b⁻Ly6C⁻ double negative (CD3⁻B220⁻Ter119⁻Ly6G⁻CD45⁺Cd11b⁻Ly6C⁻) populations and sorted using either 4- or 5-laser FACS Aria III systems. Data were analyzed using FlowJo software (Version 10, Tree Star Inc). The purity of sorted populations was >90%.

In Vitro Osteoclast Formation Assays

FACS purified populations were used immediately after sorting. 5.0×10^5 unsorted whole bone marrow or 1.0×10^4 FACS purified populations were seeded per well into 96-well plates supplemented with 5% v/v CMG14-12 supernatant (as a source of M-CSF) and 35 ng/mL RANKL. Cells were cultured for 4 days, at which point the cells were fixed and stained for TRAP per the manufacturer's instructions (Sigma). Where indicated, cells were treated with 10 µg/mL of either anti-MDL-1 (R&D, clone 226402) or IgG2a isotype control (R&D clone 54447). Fixed cells were stained with DAPI and imaged using a Cytation 5 imaging system (Biotek) prior to manual enumeration of multinucleated TRAP⁺ cells as osteoclasts.

Multiplexed Cytokine Analysis

Femurs were homogenized in mammalian tissue cell lysis buffer (Sigma) at 4 °C in sterile Bullet Blender Navy Bead Lysis Kit 1.5 mL microcentrifuge tubes (Next Advance, Troy, NY) using a Bullet Blender BBX24 (Next Advance, Troy, NY). Cell lysates were frozen at –80°C

until use for multiplexed cytokine detection. Thawed cell lysates were centrifuged twice at $4000 \times g$ for 5 minutes at 4 °C to remove debris and then subjected to multiplexed cytokine detection via the Milliplex-MAP magnetic bead-based antibody detection kits (EMD Millipore, Billerica, MA) according to manufacturer's instructions. Specifically, the 32-plex Mouse Cytokine/Chemokine Magnetic Bead Panel (MCMYTMAG-70K-PX32) or the Mouse Th17 Magnetic Bead Panel (MTH17MAG-47K) kits were used, and data were collected using the FLEXMAP 3D instrument. Measurements were corrected for total protein input as quantified by the Pierce BCA Protein Assay Kit per manufacturer's instructions and reported as either log₂ fold change in pg/mg of cytokine abundances in mice with colitis compared with controls or pg/mg normalized cytokine abundances.

Statistical Analysis

Statistical analyses were conducted using GraphPad Prism Software (Version 9). Statistical significance was assessed using the 2-tailed Student *t* test, ordinary 1-way ANOVA with post-hoc Holm-Šidák multiple comparison's test, or 2-way ANOVA with post-hoc Šidák multiple comparisons test as appropriate and as indicated in the figure legends. Differences were considered significant with a *P* value (*P* < .05). Post-hoc multiple comparisons test for significant differences within groups were only performed following a significant ANOVA *P* value (*P* < .05).

References

- Levine JS, Burakoff R. Extraintestinal manifestations of inflammatory bowel disease. *Gastroenterol Hepatol (N Y)* 2011;7:235–241.
- Ott C, Schölmerich J. Extraintestinal manifestations and complications in IBD. *Nat Rev Gastroenterol Hepatol* 2013;10:585–595.
- Oostlander AE, Bravenboer N, Sohl E, Holzmann PJ, Woude CJ van der, Dijkstra G, Stokkers PCF, Oldenburg B, Netelenbos JC, Hommes DW, Bodegraven AA van, Lips P. Dutch Initiative on Crohn and Colitis (ICC). Histomorphometric analysis reveals reduced bone mass and bone formation in patients with quiescent Crohn's disease. *Gastroenterology* 2011; 140:116–123.
- Targownik LE, Bernstein CN, Leslie WD. Inflammatory bowel disease and the risk of osteoporosis and fracture. *Maturitas* 2013;76:315–319.
- Ghosh S, Cowen S, Hannan WJ, Ferguson A. Low bone-mineral density in Crohn's disease, but not in ulcerative colitis, at diagnosis. *Gastroenterology* 1994; 107:1031–1039.
- Bernstein CN, Seeger LL, Anton PA, Artinian L, Geffrey S, Goodman W, Belin TR, Shanahan F. A randomized, placebo-controlled trial of calcium supplementation for decreased bone density in corticosteroid-using patients with inflammatory bowel disease: a pilot study. *Aliment Pharmacol Ther* 1996;10:777–786.
- Abreu MT, Geller JL, Vasiliauskas EA, Kam LY, Vora P, Martyak LA, Yang H, Hu B, Lin Y-C, Keenan G, Price J,

- Landers CJ, Adams JS, Targan SR. Treatment with infliximab is associated with increased markers of bone formation in patients with Crohn's disease. *J Clin Gastroenterol* 2006;40:55–63.
8. Miheller P, Müzes G, Rácz K, Blázovits A, Lakatos P, Herszényi L, Tulassay Z. Changes of OPG and RANKL concentrations in Crohn's disease after infliximab therapy. *Inflamm Bowel Dis* 2007;13:1379–1384.
 9. Jacquin C, Gran DE, Lee SK, Lorenzo JA, Aguila HL. Identification of multiple osteoclast precursor populations in murine bone marrow. *J Bone Miner Res* 2006;21:67–77.
 10. Muto A, Mizoguchi T, Udagawa N, Ito S, Kawahara I, Abiko Y, Arai A, Harada S, Kobayashi Y, Nakamichi Y, Penninger JM, Noguchi T, Takahashi N. Lineage-committed osteoclast precursors circulate in blood and settle down into bone. *J Bone Miner Res* 2011;26:2978–2990.
 11. Jacome-Galarza CE, Lee SK, Lorenzo JA, Aguila HL. Identification, characterization, and isolation of a common progenitor for osteoclasts, macrophages, and dendritic cells from murine bone marrow and periphery. *J Bone Miner Res* 2013;28:1203–1213.
 12. Rivollier A, Mazzorana M, Tebib J, Piperno M, Aitsiselmi T, Rabourdin-Combe C, Jurdic P, Servet-Delprat C. Immature dendritic cell transdifferentiation into osteoclasts: a novel pathway sustained by the rheumatoid arthritis microenvironment. *Blood* 2004;104:4029–4037.
 13. Moschen AR, Kaser A, Enrich B, Ludwiczek O, Gabriel M, Obrist P, Wolf AM, Tilg H. The RANKL/OPG system is activated in inflammatory bowel disease and relates to the state of bone loss. *Gut* 2005;54:479–487.
 14. Koga T, Inui M, Inoue K, Kim S, Suematsu A, Kobayashi E, Iwata T, Ohnishi H, Matozaki T, Kodama T, Taniguchi T, Takayanagi H, Takai T. Costimulatory signals mediated by the ITAM motif cooperate with RANKL for bone homeostasis. *Nature* 2004;428:758–763.
 15. Humphrey MB, Nakamura MC. A comprehensive review of immunoreceptor regulation of osteoclasts. *Clin Rev Allergy Immunol* 2016;51:48–58.
 16. Horton JE, Raisz LG, Simmons HA, Oppenheim JJ, Mergenhagen SE. Bone resorbing activity in supernatant fluid from cultured human peripheral blood leukocytes. *Science* 1972;177:793–795.
 17. Lam J, Takeshita S, Barker JE, Kanagawa O, Ross FP, Teitelbaum SL. TNF-alpha induces osteoclastogenesis by direct stimulation of macrophages exposed to permissive levels of RANK ligand. *J Clin Invest* 2000;106:1481–1488.
 18. Wei S, Kitaura H, Zhou P, Ross FP, Teitelbaum SL. IL-1 mediates TNF-induced osteoclastogenesis. *J Clin Invest* 2005;115:282–290.
 19. Khan UA, Hashimi SM, Bakr MM, Forwood MR, Morrison NA. CCL2 and CCR2 are essential for the formation of osteoclasts and foreign body giant cells. *J Cell Biochem* 2016;117:382–389.
 20. Ishii M, Egen JG, Klauschen F, Meier-Schellersheim M, Saeki Y, Vacher J, Proia RL, Germain RN. Sphingosine-1-phosphate mobilizes osteoclast precursors and regulates bone homeostasis. *Nature* 2009;458:524–528.
 21. Li X, Loberg R, Liao J, Ying C, Snyder LA, Pienta KJ, McCauley LK. A destructive cascade mediated by CCL2 facilitates prostate cancer growth in bone. *Cancer Res* 2009;69:1685–1692.
 22. Cheung R, Shen F, Phillips JH, McGeachy MJ, Cua DJ, Heyworth PG, Pierce RH. Activation of MDL-1 (CLEC5A) on immature myeloid cells triggers lethal shock in mice. *J Clin Invest* 2011;121:4446–4461.
 23. Joyce-Shaikh B, Bigler ME, Chao C-C, Murphy EE, Blumenschein WM, Adamopoulos IE, Heyworth PG, Antonenko S, Bowman EP, McClanahan TK, Phillips JH, Cua DJ. Myeloid DAP12-associating lectin (MDL)-1 regulates synovial inflammation and bone erosion associated with autoimmune arthritis. *J Exp Med* 2010;207:579–589.
 24. Shin H-S, Sarin R, Dixit N, Wu J, Gershwin E, Bowman EP, Adamopoulos IE. Crosstalk among IL-23 and DNAX activating protein of 12 kDa-dependent pathways promotes osteoclastogenesis. *J Immunol* 2015;194:316–324.
 25. Chen S-T, Lin Y-L, Huang M-T, Wu M-F, Cheng S-C, Lei H-Y, Lee C-K, Chiou T-W, Wong C-H, Hsieh S-L. CLEC5A is critical for dengue-virus-induced lethal disease. *Nature* 2008;453:672–676.
 26. Aoki N, Kimura Y, Kimura S, Nagato T, Azumi M, Kobayashi H, Sato K, Tateno M. Expression and functional role of MDL-1 (CLEC5A) in mouse myeloid lineage cells. *J Leukoc Biol* 2009;85:508–517.
 27. Singh UP, Singh NP, Murphy EA, Price RL, Fayad R, Nagarkatti M, Nagarkatti PS. Chemokine and cytokine levels in inflammatory bowel disease patients. *Cytokine* 2016;77:44–49.
 28. Neurath MF. Cytokines in inflammatory bowel disease. *Nat Rev Immunol* 2014;14:329–342.
 29. Friedrich M, Pohin M, Powrie F. Cytokine networks in the pathophysiology of inflammatory bowel disease. *Immunity* 2019;50:992–1006.
 30. Ghishan FK, Kiela PR. Advances in the understanding of mineral and bone metabolism in inflammatory bowel diseases. *Am J Physiol Gastrointest Liver Physiol* 2011;300:G191–G201.
 31. Hamdani G, Gabet Y, Rachmilewitz D, Karmeli F, Bab I, Dresner-Pollak R. Dextran sodium sulfate-induced colitis causes rapid bone loss in mice. *Bone* 2008;43:945–950.
 32. Harris L, Senagore P, Young VB, McCabe LR. Inflammatory bowel disease causes reversible suppression of osteoblast and chondrocyte function in mice. *Am J Physiol Gastrointest Liver Physiol* 2009;296:G1020–G1029.
 33. Irwin R, Raehtz S, Parameswaran N, McCabe LR. Intestinal inflammation without weight loss decreases bone density and growth. *Am J Physiol Regul Integr Comp Physiol* 2016;311:R1149–R1157.
 34. Melgar S, Bjursell M, Gerdin A-K, Svensson L, Michaëlsson E, Bohlooly-Y M. Mice with experimental colitis show an altered metabolism with decreased metabolic rate. *Am J Physiol Gastrointest Liver Physiol* 2007;292:G165–G172.

35. DeBoer MD, Steinman J, Li Y. Partial normalization of pubertal timing in female mice with DSS colitis treated with anti-TNF- α antibody. *J Gastroenterol* 2012; 47:647–654.
36. Ke K, Chen TH-P, Arra M, Mbalaviele G, Swarnkar G, Abu-Amer Y. Attenuation of NF- κ B in intestinal epithelial cells is sufficient to mitigate the bone loss comorbidity of experimental mouse colitis. *J Bone Miner Res* 2019; 34:1880–1893.
37. Oz HS, Ebersole JL. A novel murine model for chronic inflammatory alveolar bone loss. *J Periodontal Res* 2010; 45:94–99.
38. Lin CL, Moniz C, Chambers TJ, Chow J. Colitis causes bone loss in rats through suppression of bone formation. *Gastroenterology* 1996;111:1263–1271.
39. Ciucci T, Ibáñez L, Boucoiran A, Birgy-Barelli E, Pène J, Abou-Ezzi G, Arab N, Rouleau M, Hébuterne X, Yssel H, Blin-Wakkach C, Wakkach A. Bone marrow Th17 TNF α cells induce osteoclast differentiation, and link bone destruction to IBD. *Gut* 2015;64:1072–1081.
40. Byrne FR, Morony S, Warmington K, Geng Z, Brown HL, Flores SA, Fiorino M, Yin SL, Hill D, Porkess V, Duryea D, Pretorius JK, Adamu S, Manoukian R, Manoukian R, Danilenko DM, Sarosi I, Lacey DL, Kostenuik PJ, Senaldi G. CD4+CD45RB^{hi} T cell transfer induced colitis in mice is accompanied by osteopenia which is treatable with recombinant human osteoprotegerin. *Gut* 2005;54:78–86.
41. Ashcroft AJ, Cruickshank SM, Croucher PL, Perry MJ, Rollinson S, Lippitt JM, Child JA, Dunstan C, Felsburg PJ, Morgan GJ, Carding SR. Colonic dendritic cells, intestinal inflammation, and T cell-mediated bone destruction are modulated by recombinant osteoprotegerin. *Immunity* 2003;19:849–861.
42. Ibáñez L, Abou-Ezzi G, Ciucci T, Amiot V, Belaïd N, Obino D, Mansour A, Rouleau M, Wakkach A, Blin-Wakkach C. Inflammatory osteoclasts prime TNF α -producing CD4+ T cells and express CX3 CR1. *J Bone Miner Res* 2016;31:1899–1908.
43. Cohen SL, Moore AM, Ward WE. Interleukin-10 knockout mouse: a model for studying bone metabolism during intestinal inflammation. *Inflamm Bowel Dis* 2004; 10:557–563.
44. Trottier MD, Irwin R, Li Y, McCabe LR, Fraker PJ. Enhanced production of early lineages of monocytic and granulocytic cells in mice with colitis. *Proc Natl Acad Sci U S A* 2012;109:16594–16599.
45. Powrie F, Leach MW, Mauze S, Menon S, Caddle LB, Coffman RL. Inhibition of Th1 responses prevents inflammatory bowel disease in scid mice reconstituted with CD45RB^{hi} CD4+ T cells. *Immunity* 1994;1:553–562.
46. Raffatellu M, George MD, Akiyama Y, Hornsby MJ, Nuccio S-P, Paixao TA, Butler BP, Chu H, Santos RL, Berger T, Mak TW, Tsolis RM, Bevins CL, Solnick JV, Dandekar S, Bäumlér AJ. Lipocalin-2 resistance confers an advantage to *Salmonella enterica* serotype Typhimurium for growth and survival in the inflamed intestine. *Cell Host Microbe* 2009;5:476–486.
47. Charles JF, Hsu L-Y, Niemi EC, Weiss A, Aliprantis AO, Nakamura MC. Inflammatory arthritis increases mouse osteoclast precursors with myeloid suppressor function. *J Clin Invest* 2012;122:4592–4605.
48. Chong SZ, Evrard M, Devi S, Chen J, Lim JY, See P, Zhang Y, Adrover JM, Lee B, Tan L, Li JLY, Liong KH, Phua C, Balachander A, Boey A, Liebl D, Tan SM, Chan JKY, Balabanian K, Harris JE, Bianchini M, Weber C, Duchene J, Lum J, Poidinger M, Chen Q, Rénia L, Wang C-I, Larbi A, Randolph GJ, Weninger W, Looney MR, Krummel MF, Biswas SK, Ginhoux F, Hidalgo A, Bachelier F, Ng LG. CXCR4 identifies transitional bone marrow premonocytes that replenish the mature monocyte pool for peripheral responses. *J Exp Med* 2016;213:2293–2314.
49. González-Domínguez érika, Samaniego R, Flores-Sevilla JL, Campos-Campos SF, Gómez-Campos G, Salas A, Campos-Peña V, Corbí ÁL, Sánchez-Mateos P, Sánchez-Torres C. CD163L1 and CLEC5A discriminate subsets of human resident and inflammatory macrophages in vivo. *J Leukocyte Biol* 2015; 98:453–466.
50. Martin JC, Chang C, Boschetti G, Ungaro R, Giri M, Grout JA, Gettler K, Chuang L, Nayar S, Greenstein AJ, Dubinsky M, Walker L, Leader A, Fine JS, Whitehurst CE, Mbow ML, Kugathasan S, Denson LA, Hyams JS, Friedman JR, Desai PT, Ko HM, Laface I, Akturk G, Schadt EE, Salmon H, Gnjjatic S, Rahman AH, Merad M, Cho JH, Kenigsberg E. Single-cell analysis of Crohn's disease lesions identifies a pathogenic cellular module associated with resistance to anti-TNF therapy. *Cell* 2019;178:1493–1508.e20.
51. Massimino L, Lamparelli LA, Houshyar Y, D'Alessio S, Peyrin-Biroulet L, Vetrano S, Danese S, Ungaro F. The Inflammatory Bowel Disease Transcriptome and Meta-transcriptome Meta-Analysis (IBD TaMMA) framework. *Nat Comput Sci* 2021;1:511–515.
52. Aune TM, Crooke PS, Patrick AE, Tossberg JT, Olsen NJ, Spurlock CF 3rd. Expression of long non-coding RNAs in autoimmunity and linkage to enhancer function and autoimmune disease risk genetic variants. *J Autoimmun* 2017;81:99–109.
53. Aschenbrenner D, Quaranta M, Banerjee S, Ilott N, Jansen J, Steere B, Chen Y-H, Ho S, Cox K, Arancibia-Cárcamo CV, Coles M, Gaffney E, Travis SP, Denson L, Kugathasan S, Schmitz J, Powrie F, Sansom SN, Uhlig HH. Deconvolution of monocyte responses in inflammatory bowel disease reveals an IL-1 cytokine network that regulates IL-23 in genetic and acquired IL-10 resistance. *Gut* 2021;70:1023–1036.
54. Inui M, Kikuchi Y, Aoki N, Endo S, Maeda T, Sugahara-Tobinai A, Fujimura S, Nakamura A, Kumanogoh A, Colonna M, Takai T. Signal adaptor DAP10 associates with MDL-1 and triggers osteoclastogenesis in cooperation with DAP12. *Proc Natl Acad Sci U S A* 2009; 106:4816–4821.
55. Kim HK, Sierra MDLL, Williams CK, Gulino AV, Tosato G. G-CSF down-regulation of CXCR4 expression identified as a mechanism for mobilization of myeloid cells. *Blood* 2006;108:812–820.
56. Petit I, Szyper-Kravitz M, Nagler A, Lahav M, Peled A, Habler L, Ponomarev T, Taichman RS, Arenzana-

- Seisededos F, Fujii N, Sandbank J, Zipori D, Lapidot T. G-CSF induces stem cell mobilization by decreasing bone marrow SDF-1 and up-regulating CXCR4. *Nat Immunol* 2002;3:687–694.
57. Herman S, Müller RB, Krönke G, Zwerina J, Redlich K, Hueber AJ, Gelse H, Neumann E, Müller-Ladner U, Schett G. Induction of osteoclast-associated receptor, a key osteoclast costimulation molecule, in rheumatoid arthritis. *Arthritis Rheum* 2008;58:3041–3050.
 58. Ochi S, Shinohara M, Sato K, Gober H-J, Koga T, Kodama T, Takai T, Miyasaka N, Takayanagi H. Pathological role of osteoclast costimulation in arthritis-induced bone loss. *Proc Natl Acad Sci U S A* 2007;104:11394–11399.
 59. Dresner-Pollak R, Gelb N, Rachmilewitz D, Karmeli F, Weinreb M. Interleukin 10-deficient mice develop osteopenia, decreased bone formation, and mechanical fragility of long bones. *Gastroenterology* 2004;127:792–801.
 60. Radhakrishnan VM, Gilpatrick MM, Parsa NA, Kiela PR, Ghishan FK. Expression of Cav1.3 calcium channel in the human and mouse colon: posttranscriptional inhibition by IFN γ . *Am J Physiol Gastrointest Liver Physiol* 2017;312:G77–G84.
 61. Radhakrishnan VM, Ramalingam R, Larmonier CB, Thurston RD, Laubitz D, Kiela MTM, McFadden RMT, O MK, Kiela PR, Ghishan FK. Post-translational loss of renal TRPV5 calcium channel expression, Ca(2⁺) wasting, and bone loss in experimental colitis. *Gastroenterology* 2013;145:613–624.
 62. Thurston RD, Larmonier CB, Majewski PM, Ramalingam R, Midura-Kiela M, Laubitz D, Vandewalle A, Besselsen DG, Mühlbauer M, Jobin C, Kiela PR, Ghishan FK. Tumor necrosis factor and interferon-gamma down-regulate Klotho in mice with colitis. *Gastroenterology* 2010;138:1384–1394, 1394.e1–2.
 63. Gobert AP, Finley JL, Latour YL, Asim M, Smith TM, Verriere TG, Barry DP, Allaman MM, Delgado AG, Rose KL, Calcutt MW, Schey KL, Sierra JC, Piazuelo MB, Mirmira RG, Wilson KT. Hypusination orchestrates the antimicrobial response of macrophages. *Cell Reports* 2020;33:108510.
 64. Hardbower DM, Asim M, Luis PB, Singh K, Barry DP, Yang C, Steeves MA, Cleveland JL, Schneider C, Piazuelo MB, Gobert AP, Wilson KT. Ornithine decarboxylase regulates M1 macrophage activation and mucosal inflammation via histone modifications. *Proc Natl Acad Sci U S A* 2017;114:E751–E760.
 65. Rivera-Chávez F, Zhang LF, Faber F, Lopez CA, Byndloss MX, Olsan EE, Xu G, Velazquez EM, Lebrilla CB, Winter SE, Bäumlér AJ. Depletion of butyrate-producing clostridia from the gut microbiota drives an aerobic luminal expansion of salmonella. *Cell Host Microbe* 2016;19:443–454.
 66. Dieleman LA, Palmen MJ, Akol H, Bloemena E, Peña AS, Meuwissen SG, Rees EPV. Chronic experimental colitis induced by dextran sulphate sodium (DSS) is characterized by Th1 and Th2 cytokines. *Clin Exp Immunol* 1998;114:385–391.
 67. Kennedy RJ, Hoper M, Deodhar K, Erwin PJ, Kirk SJ, Gardiner KR. Interleukin 10-deficient colitis: new similarities to human inflammatory bowel disease. *Brit J Surg* 2000;87:1346–1351.
 68. Bouxsein ML, Boyd SK, Christiansen BA, Guldberg RE, Jepsen KJ, Müller R. Guidelines for assessment of bone microstructure in rodents using micro-computed tomography. *J Bone Miner Res* 2010;25:1468–1486.
 69. Dempster DW, Compston JE, Drezner MK, Glorieux FH, Kanis JA, Malluche H, Meunier PJ, Ott SM, Recker RR, Parfitt AM. Standardized nomenclature, symbols, and units for bone histomorphometry: a 2012 update of the report of the ASBMR Histomorphometry Nomenclature Committee. *J Bone Miner Res* 2013;28:2–17.

Received February 26, 2022. Accepted July 5, 2022.

Correspondence

Address correspondence to: Dr Jim Cassat, Division of Pediatric Infectious Diseases, Department of Pediatrics, Vanderbilt University Medical Center, 1035 Light Hall, 2215-B Garland Ave, Nashville, TN, 37232. e-mail: jim.cassat@vumc.org; tel: (615) 936-6494.

Acknowledgment

The authors thank Nicole Putnam for assistance generating pilot data for these studies, Margaret Allaman for technical assistance with Luminex multiplexed cytokine detection, and Jennifer Marvin-Peek for critical review on the manuscript.

CRedit Authorship Contributions

Christopher T. Peek (Conceptualization: Supporting; Data curation: Lead; Formal analysis: Equal; Investigation: Lead; Methodology: Lead; Writing – original draft: Lead; Writing – review & editing: Equal)

Caleb A. Ford (Investigation: Supporting; Writing – review & editing: Supporting)

Kara R. Eichelberger (Investigation: Supporting; Writing – review & editing: Supporting)

Justin Jacobse (Investigation: Supporting; Methodology: Supporting; Writing – review & editing: Supporting)

Teresa P. Torres (Investigation: Supporting; Writing – review & editing: Supporting)

Damian Maseda (Investigation: Supporting; Writing – review & editing: Supporting)

Yvonne L. Latour (Investigation: Supporting; Writing – review & editing: Supporting)

M. Blanca Piazuelo (Writing – review & editing: Supporting; Blinded histopathologic analysis: Lead)

Joshua R. Johnson (Methodology: Supporting; Writing – review & editing: Supporting)

Mariana X. Byndloss (Conceptualization: Supporting; Funding acquisition: Supporting; Resources: Supporting; Supervision: Supporting; Writing – review & editing: Supporting; Blinded histopathologic analysis: Supporting)

Keith T. Wilson (Conceptualization: Supporting; Funding acquisition: Supporting; Resources: Supporting; Supervision: Supporting; Writing – review & editing: Supporting)

Jeffrey C. Rathmell (Conceptualization: Supporting; Funding acquisition: Supporting; Resources: Supporting; Supervision: Supporting; Writing – review & editing: Supporting)

Jeremy A. Goettel (Conceptualization: Supporting; Funding acquisition: Supporting; Resources: Supporting; Supervision: Supporting; Writing – review & editing: Supporting)

James Cassat, M.D., Ph.D. (Conceptualization: Lead; Formal analysis: Equal; Funding acquisition: Lead; Investigation: Supporting; Project administration: Lead; Resources: Lead; Supervision: Lead; Writing – original draft: Supporting; Writing – review & editing: Equal)

Conflicts of interest

This author discloses the following: Dr Jeffrey Rathmell is a founder, scientific advisory board member, and stockholder of Sitryx Therapeutics, a scientific advisory board member and stockholder of Caribou Biosciences, a member of the scientific advisory board of Nirogy Therapeutics, has consulted for Merck, Pfizer, and Mitobridge within the past 3 years, and has received research support from Incyte Corp, Calithera Biosciences, and Tempest Therapeutics. The remaining authors disclose no conflicts.

Funding

The Vanderbilt Translational Pathology Shared Resource is supported by the National Cancer Institute (NCI)/National Institutes of Health (NIH) Cancer Center Support Grant 5P30 CA68485-19. James E. Cassat was supported by a Career Award for Medical Scientists from the Burroughs Wellcome Fund, pilot funding from the Vanderbilt University Medical Center Digestive Disease Research Center grant P30DK058404, and Senior Research Award #709139 from the Crohn's and Colitis Foundation. Christopher T. Peek was supported by NIH grant T32M007347 and is supported by NIH grant F30DK120114-04. Caleb A. Ford was supported by NIH grant T32M007347 and is supported by NIH grant F30A138424. Kara R. Eichelberger is supported by NIH grant 2T32AI095202. Joshua R. Johnson is supported by

The Academy Ter Meulen Grant from the Royal Netherlands Academy of Arts and Sciences and the Cultural Foundation Grant from Prince Bernhard Cultural Foundation. Yvonne L. Latour was supported by NIH grant T32AI138932. Jeremy A. Goettel is supported by NIH grant R03DK123489. Keith T. Wilson is supported by Senior Research Award #703003 from the Crohn's and Colitis Foundation, NIH grant R01DK128200, VA Merit Review grant I01CX002171, and Department of Defense Award W81XWH-21-1-0617. Mariana X. Byndloss is supported by pilot funding from the Vanderbilt University Medical Center Digestive Disease Research Center grant P30DK058404, by United States-Israel Binational Science Foundation grant #2019136, and by V Scholar grant V2020-013 from The V Foundation for Cancer Research. Jeffrey C. Rathmell is supported by NIH R01 DK105550.